INSTITUTE OF PHYSICS PUBLISHING REPORTS ON PROGRESS IN PHYSICS

Rep. Prog. Phys. **66** (2003) 583–632 PII: S0034-4885(03)31847-0

Interference and interactions in open quantum dots

J P Bird[1], R Akis[1], D K Ferry[1], A P S de Moura[2], Y-C Lai[1,2] and K M Indlekofer[1]

[1] Nanostructures Research Group, Department of Electrical Engineering, Arizona State University, Tempe, AZ 85287-5706, USA
[2] Department of Mathematics, Arizona State University, Tempe, AZ 85287-1804, USA

Received 22 January 2003
Published 14 March 2003
Online at stacks.iop.org/RoPP/66/583

Abstract

In this report, we review the results of our joint experimental and theoretical studies of electron-interference, and interaction, phenomena in open electron cavities known as quantum dots. The transport through these structures is shown to be heavily influenced by the remnants of their discrete density of states, elements of which remain resolved in spite of the strong coupling that exists between the cavity and its reservoirs. The experimental signatures of this density of states are discussed at length in this report, and are shown to be related to characteristic wavefunction scarring, involving a small number of classical orbits. A semiclassical analysis of this behaviour shows it to be related to the effect of dynamical tunnelling, in which electrons are injected into the dot tunnel through classically forbidden regions of phase space, to access isolated regular orbits. The dynamical tunnelling gives rise to the formation of long-lived quasi-bound states in the open dots, and the many-body implications associated with electron charging at these resonances are also explored in this report.

Contents

Nomenclature

2DEG	two-dimensional electron gas
A_d	quantum-dot area
B	magnetic field
B_c	correlation magnetic field
c_n	wavefunction expansion coefficient
$c^+_{k\sigma}/c_{k\sigma}$	creation/annihilation operators
Δ	average level spacing
E	energy
E_F	Fermi energy
E_0	resonance energy
$f(E)$	Fermi–Dirac distribution function
G	quantum-dot conductance
γ	logarithmic conductance prefactor
Γ	energy width of interaction resonance
k	electron wavenumber
l	transport mean free path
L	effective dot size
λ	Maslov index
λ_F	Fermi wavelength
m^*	electron effective mass
μ	two-dimensional electron gas mobility
μ_k	electrochemical potential of mode with wavenumber k
N	number of one-dimensional sub-bands
n	quantum-dot eigenstate number
n_b	number of coherent skipping-orbit bounces
n_s	two-dimensional electron gas carrier density
T_0	activation temperature
ϕ_n	closed-dot eigenfunctions
r_c	cyclotron radius
S	classical-orbit action
S_eff	effective action
σ	spin index
ψ	quantum-dot wavefunction
T	temperature
T^*	effective electron temperature
T_0	activation temperature
τ_ϕ	phase-breaking time
U, U^ex	Hartree, exchange potentials
V_g	gate voltage
ω	orbit stability angle

1. Introduction

In the field of research known as mesoscopic physics, interest lies in studying the manner in which the electronic properties of materials are modified by confining their charge carriers on distances comparable to the fundamental length scales for transport (for a number of excellent reviews in this area, see [1–4]). One of the simplest low-dimensional electron systems is the high-mobility two-dimensional electron gas (2DEG) that forms at the interface between two lattice-matched semiconductors (such as GaAs and AlGaAs), when they are grown on top of each other by molecular-beam epitaxy (see figure 1). The strong interfacial confinement that arises in these systems quantizes the energy for motion transverse to the heterointerface, modifying the nature of the carrier interactions, and the form of the density of states. As a result, the electrical properties of 2DEG systems are found to be quite distinct from those of bulk materials. Further confining the electron motion in one additional direction, it is possible to realize a quasi-one-dimensional quantum wire, in which electrons may move freely along the wire axis, while their transverse motion is quantized into a small number of sub-bands, or channels. In the absence of scattering within the wire, and in the limit of small applied source-drain bias, an equipartition of current among the occupied sub-bands causes the conductance

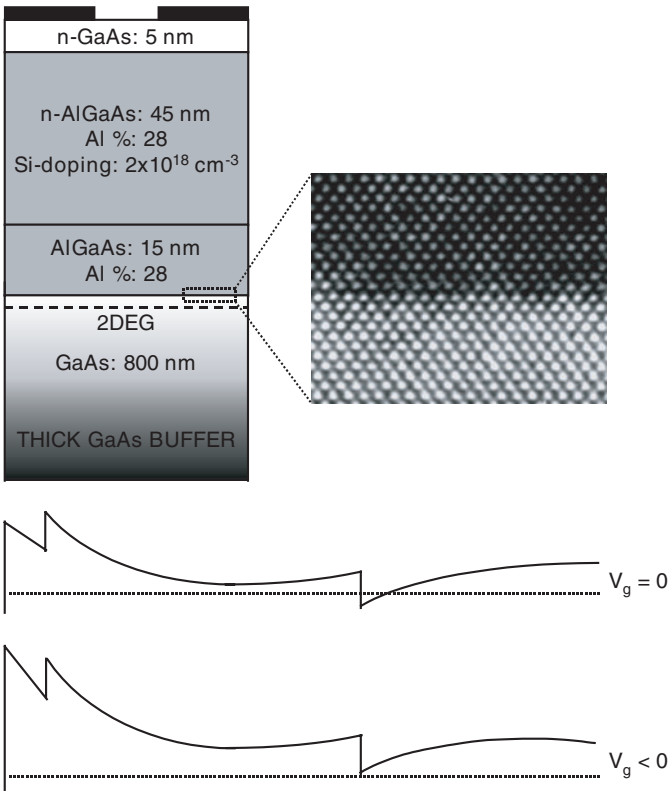

Figure 1. The upper part of the figure shows a cross section of the typical components of a GaAs/AlGaAs heterojunction, along with an SEM image of the associated heterointerface. The lower panel shows the influence of a gate voltage on the conduction-band profile of the heterojunction.

of such quantum point-contacts to be quantized according to [5]:

$$G = \frac{2e^2}{h}N, \tag{1}$$

where N is the number of occupied channels and simply corresponds to the number of sub-bands whose threshold energies lie below the Fermi energy. In addition to the conductance quantization defined in equation (1), and dependent on the ratio of the wire dimensions to the characteristic transport length scales, other phenomena that may occur in quantum wires include universal conductance fluctuations, quenching of the Hall effect, and Luttinger-liquid behaviour, all of which have been widely studied in recent years (for a thorough review of many of these topics, see [5]).

Quantum dots may be viewed as the ultimate limit of bandstructure engineering and are realized when electron motion is confined in all three directions, on length scales comparable to the coherence length. An important result of this strong confinement is that the energy spectrum of the electrons is quantized into a discrete set of levels, that may be modified by the application of a magnetic field, or some appropriate gate voltage. The electrical properties of these artificial atoms are strongly influenced by the discrete form of their density of states [6,7] and there is much interest in their potential for application in a range of future technologies. Quantum dots have been proposed, for example, for use as qubits in quantum computing [8,9], and have been used to provide demonstrations of quantum-cellular automata [10] and single-photon detectors [11]. In these applications, a quantitative understanding of the details of electron transport in the dots is required, and it is this need that serves as the motivation for this report, where we review our recent work in this particular problem.

When discussing transport through quantum dots, it is possible to identify two distinct regimes of behaviour, dependent on the strength of the coupling between the dot and its current reservoirs. In weakly coupled quantum dots, current flow involves a process in which electrons tunnel through the dot, and, at sufficiently low temperatures, the charging energy associated with the addition of a single electron to the dot can be very much larger than the thermal energy. In this so-called Coulomb-blockade regime, current flow occurs by the process of single-electron tunnelling, which is comprehensively reviewed in [3,6,7]. Of interest here, however, is the problem of transport in open quantum dots, in which the coupling between the dot and its reservoirs is provided by means of quantum-point-contact leads, each of which supports at least one propagating mode. The Coulomb-blockade effect is washed out in such structures [12,13], in which the transport instead is strongly influenced by the interference of electrons confined within the dots. In this sense, these dots may be viewed as the quantum analog of classical wave-scattering systems, such as microwave cavities [14,15], fluid systems [16], and semiconductor lasers [17]. At the same time, the analysis of transport through these structures is particularly amenable to semiclassical methods, in which path integrals over classical trajectories are used to calculate their conductance (for a recent review, see [18]).

In this review, we consider the development of quantum-mechanical and semiclassical descriptions of transport in open quantum dots, whose predictions are consistent with each other, and with the results of experimental studies. A crucial feature of these dots is found to be a non-uniform broadening of their eigenstates, which arises when the dot is opened to its reservoirs. Certain eigenstates of the initially-closed-dot are found to develop only a very small broadening as a result of this coupling, and therefore persist to give rise to measurable transport results. These states correspond to the eigenfunctions of the original system which are scarred by the signature of periodic orbits, and which exhibit a weak overlap with the dot leads. If a magnetic field is applied perpendicular to the plane of the quantum dot, or its potential profile is modified by means of a suitable gate voltage, the discrete states may be swept past the Fermi level, giving rise to reproducible oscillations in the conductance that may be observed at low

temperatures. An important feature of the wavefunction scars is that they recur periodically as the magnetic field, or the gate voltage, is varied, and our analysis shows that this behaviour gives rise to very specific frequency components in the associated conductance oscillations. A semiclassical analysis of this behaviour indicates that the scars are associated with the dynamical tunnelling of electrons through classically forbidden regions of phase space, onto isolated periodic orbits. Quantization of the action associated with these orbits is shown to give rise to a series of resonance conditions, which account for the observed periodicity of the conductance oscillations seen in experiment. While it has been common in the literature thus far to assume that the transport is dominated by chaotic trajectories, classically accessible to electrons injected into the dot, our analysis demonstrates that the dominant mechanism is instead very different.

In addition to considering the connection of the semiclassical and quantum-mechanical descriptions of transport in these structures, we also explore the importance of many-body effects for transport. Experimental studies of the temperature-dependent transport in these dots reveal evidence for behaviour, analogous to a metal–insulator transition, the characteristic signature of which is a logarithmic variation of the conductance at low temperatures. Similar logarithmic variations are a well-known signature of the Kondo effect, and we suggest that similar physics may even be at play here. The point to note is that a general requirement for the observation of the Kondo effect is the realization of some localized region of charge, which can interact with a continuum of states. In the open dots that we study, such localized charge should be realized by the isolated KAM islands which represent classically inaccessible orbits. To explore the many-body consequences of this tunnelling, we therefore develop a theoretical model which is based upon the assumption that the electron-interaction strength in the dots can be peaked at certain energies, corresponding to the resonant conditions for the dynamical tunnelling. This model reveals the presence of low-temperature, interaction-induced, corrections to the conductance of the open dots.

The organization of this review is as follows. In the next section, we describe the fabrication of the quantum-dot devices, and describe the basic electrical characteristics. In section 3, we discuss the details of transport at very-low temperatures, where the influence of thermal smearing and decoherence is minimal, and where the conductance can be viewed as providing a spectroscopy of the density of states of the open dot. It is here that we explore the quantum-mechanical and semiclassical interpretations of transport in these structures, emphasizing the role of non-uniform level broadening, introduced by the environmental coupling to the dots, and considering its connection to the issue of dynamical tunnelling. In section 4, we discuss how quantum effects in the transport are modified at higher temperatures, and present evidence for a metal–insulator transition that is seen in the conductance below a degree kelvin. We suggest that this behaviour is associated with the increased importance of electron-interactions in these strongly confined structures, and present a many-body based transport model to account for our observations. Our conclusions are then discussed in section 5.

2. Device fabrication and basic characteristics

2.1. Device fabrication

For the transport studies that we discuss, the split-gate technique [19] is the approach of choice for the fabrication of quantum dots, and the basic principles of this method are shown in figure 2. In this approach, metal gates with a fine-line pattern defined by electron-beam lithography are formed on the surface of a GaAs/AlGaAs heterojunction (figure 2, top). The application of a negative bias to the gates depletes the regions of electron gas underneath them, by raising the

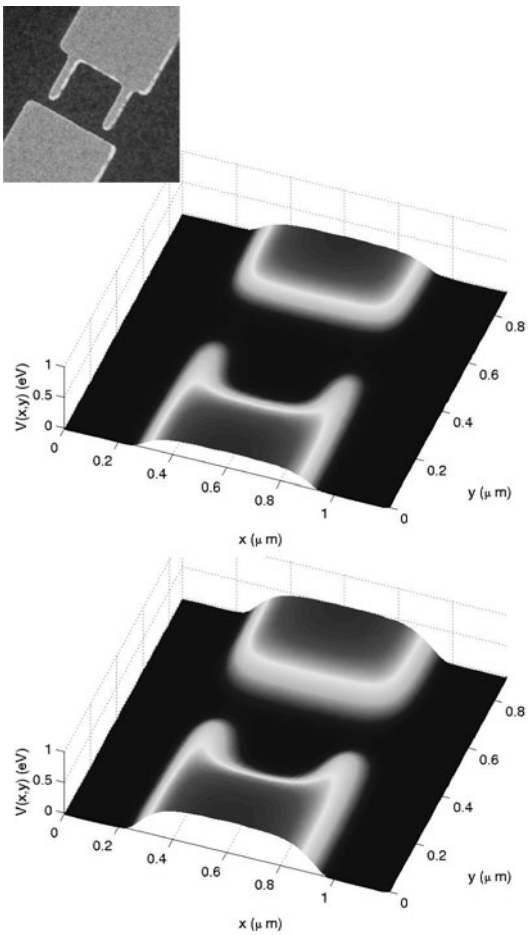

Figure 2. Top panel: scanning electron micrograph of a split-gate quantum dot with a 1 μm cavity. Lower panels: calculated potential profiles at two gate voltages. The gate voltage is more negative in the lowest panel.

local conduction-band edge above the Fermi level (see figure 1), thereby forming a quantum dot whose leads are defined by means of quantum-point-contacts (figure 2, top). The use of electron-beam lithography to define the gate pattern allows the realization of sub-micron sized dots, whose size is therefore comparable to the spatial extent of the short range potential fluctuations in the underlying 2DEG [20]. The fluctuations are associated with the statistical distribution of donors in the AlGaAs layer, and numerical studies suggest that minimum-energy considerations may cause the ionization of these donors to order into a quasi-lattice structure [21]. In the presence of the resulting weak disorder, electronic motion within the dots should therefore be predominantly ballistic in nature, with large-angle scattering events being restricted to their confining walls. At least to first order, the dot geometry is determined by the lithographic pattern of the gates, and the great advantage of this technique is the *in situ* control of the dot profile that can be achieved, simply by varying the gate voltage (V_g). These concepts are illustrated in figure 2, where we show a pair of self-consistently computed [22] potential profiles for a split-gate dot. The two different profiles are computed for different values of the gate voltage, and from a comparison of these plots we see that the effect of making the gate

Table 1. Some key parameters for the different quantum-dots studied here.

n_s (10^{15} m^{-2})	μ (m^2 Vs^{-1})	l (μm)	L (μm)	E_F (meV)	λ_F (nm)	Δ/k_B (K)	N_d
4.0–5.5	36–78	4–9	0.2–1.8	14–20	35–40	0.03–1	160–1800

n_s: two-dimensional-electron-gas carrier density.
μ: two-dimensional-electron-gas mobility.
l: two-dimensional mean free path.
L: effective dot size inferred from periodicity of Aharonov–Bohm oscillations in the edge state regime.
E_F: two-dimensional-electron-gas Fermi energy.
λ_F: two-dimensional-electron-gas Fermi wavelength.
Δ/k_B: quantum-dot average level spacing. $\Delta \equiv 2\pi\hbar^2/m^*A_d$, where $A_d = L^2$ is the dot area.
N_d: electron number in the dot. $N_d \equiv n_s L^2$.

voltage more negative is to narrow the width of the point-contact leads, and to reduce the size of the central dot itself. This is basically a consequence of the increased fringing fields, which develop around the gate edges as V_g is made more negative. Note from these plots how the split-gate approach gives rise to dots with soft walls.

In table 1, we summarize the material characteristics, and the device dimensions, of the various quantum-dot structures that we consider in this review. At the low temperatures that we consider here, the high mobility of the 2DEG sample ensures that the transport mean free path is significantly larger than the size of the dots, indicating that transport within them should be close to the ballistic limit. Another important feature to note is that the Fermi wavelength of the electrons is typically of order 40 nm, and so can approach within an order of magnitude of the dot size. We will see further below that this also has important consequences for the transport behaviour exhibited by these structures. As can be seen in table 1, the electron number in these dots ranges from several thousand in the largest structures, to a few hundred in the smallest. Further below (section 4.2), we will consider the potential implications of the many-body interactions that arise between these electrons for the analysis of transport through open dots. Also shown in table 1 are typical values for the average level spacing (Δ), which may be thought of as a rough measure of the characteristic level spacing in the dots.

2.2. Basic experimental observations

In figure 3, we show the results of measurements of the magneto–resistance of an open quantum dot, at a series of different gate voltages. (These measurements were performed with the sample mounted in a dilution refrigerator, and with the magnetic field applied perpendicular to the plane of the 2DEG.) The average dot resistance is less than 26 kΩ in each of the curves, indicating that its leads support at least one propagating mode, and that it may be considered to be open over the entire range of gate voltage shown. As expected, the average resistance of the dot increases as the gate voltage is made more negative, a trend which is accompanied by a dramatic evolution of the structure in the magneto–resistance. Dense fluctuations emerge at low magnetic fields ($<$2 T), while isolated resonances develop at higher fields. This behaviour can be seen more clearly in figure 4, in which we show a single magneto–resistance curve, measured at a fixed gate voltage. The insets to this figure serve to illustrate that the noise-like structure in the magneto–resistance is, in fact, quite reproducible. In the high-field inset, the resistance clearly oscillates periodically with magnetic field, and the origin of this behaviour is well understood [5]. At such high magnetic fields, the cyclotron radius of the electrons is very much smaller than the dot size and current is carried by a fixed number of edge states [23].

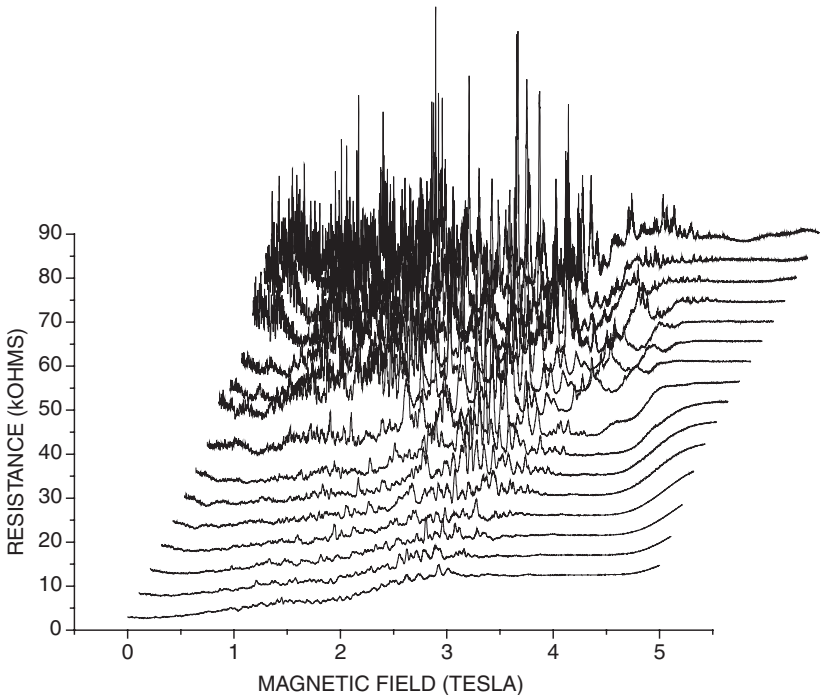

Figure 3. Magneto–resistance of a 1 μm split-gate quantum dot, at a series of different gate voltages. The gate voltage becomes more negative from front to back. The cryostat temperature is 0.01 K.

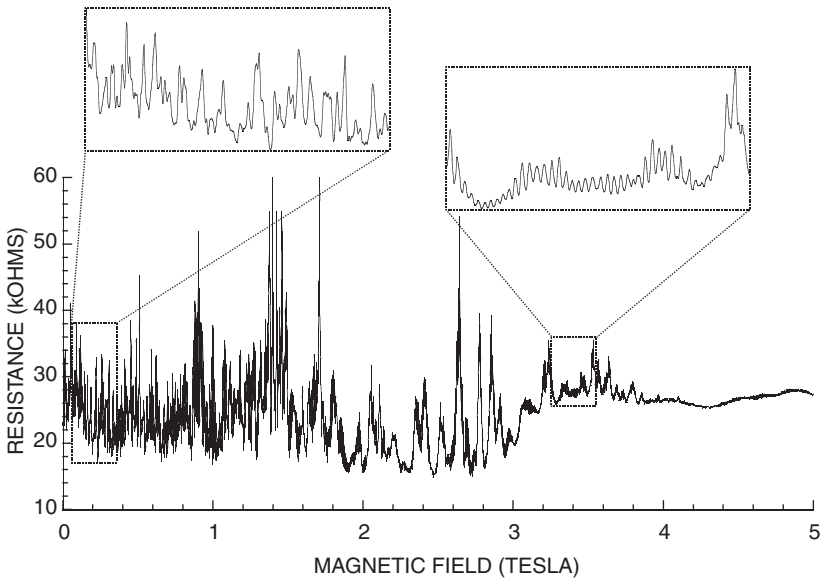

Figure 4. Magneto–resistance of a 1 μm split-gate quantum dot, at a fixed gate voltage, showing the detailed evolution of its structure with magnetic field.

These may be viewed as the quantum-mechanical analogue of classical skipping-orbits, and the various features observed in the magneto–resistance in this regime can be ascribed to dot-induced interference of the edge states [24]. The periodic oscillations at high magnetic fields (>3 T) are understood to result from an Aharonov–Bohm effect, involving edge states trapped within the dot, and allow a reasonable estimate of the dot size to be obtained. This behaviour has been discussed in detail in [25, 26], and will not be further considered here. Rather, we focus on the behaviour observed at lower fields (<1 T), where the magnetic field provides only a perturbation to the intrinsic electron dynamics in the dot. As can be seen in figure 4, the magneto–resistance in this regime shows dense fluctuations, which are dominated by a small number of frequency components (see the low-field inset). While the detailed origin of these fluctuations will be discussed below, they may basically be understood to result from the interference of electron partial waves that are generated when the electron is multiply scattered from the walls of the dot. Typical of most interference effects (for a recent review, see [27]), the fluctuations are washed out when the temperature is increased above a few degrees kelvin, as we illustrate in figure 5.

Fluctuations in the resistance may also be generated by varying the voltage applied to the split gates of the dot, as we illustrate in figure 6. This shows the gate-voltage characteristic of a typical dot, at two different temperatures and in the absence of any applied magnetic field.

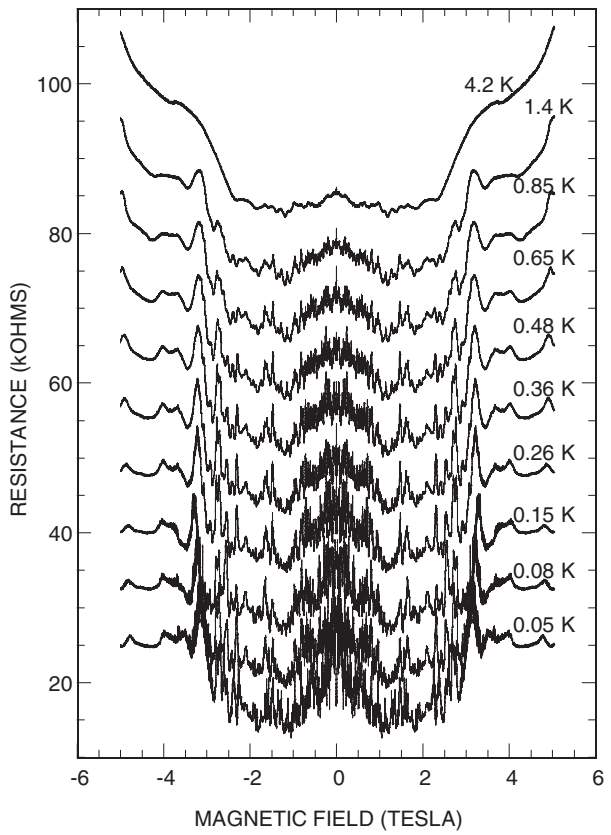

Figure 5. Temperature dependence of the magneto–resistance of a 1 μm split-gate quantum dot. Successive curves are shifted upwards from each other.

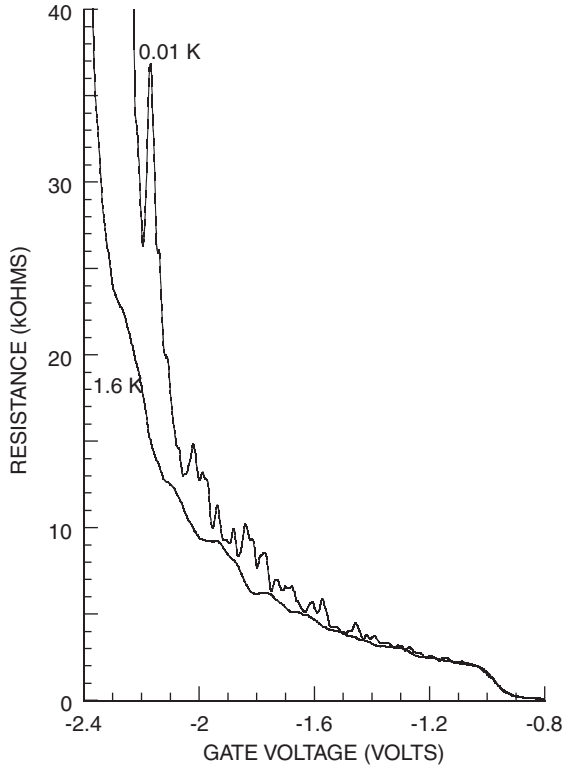

Figure 6. Gate-voltage-dependent variation of the resistance of a 1-μm split-gate quantum dot, at two different temperatures.

At 1.6 K, the resistance varies almost monotonically with gate voltage, and shows evidence for plateau features related to conductance quantization in the point-contact leads. At 0.01 K, however, the resistance develops an oscillatory behaviour, and in the inset to figure 6 we show the conductance fluctuations obtained by subtracting the background variation from the raw data. Once again, there is clearly a dominant periodicity to these fluctuations, and in the sections that follow we provide a detailed interpretation of the origin of this behaviour.

3. Transmission as a probe of the density of states

In isolated quantum dots, containing just a few electrons, it is well known that the transport can be strongly influenced by the discrete energy spectrum that is induced by confining electrons in the dot [6, 28–30]. When the dot is opened to its external reservoirs, however, it is often (wrongly) assumed that all details of this level spectrum are washed out completely. In this section of our review, we demonstrate that the reproducible conductance fluctuations discussed above provide a direct signature of those dot states that remain resolvable, even when the dot is very strongly coupled to its external reservoirs. Since this behaviour may seem surprising to some, we also provide several examples to show that the persistence of eigenstates in these dots can basically be viewed as a quantum-mechanical manifestation of the generic classical phenomenon of wave trapping.

3.1. The persistence of eigenstates in open quantum dots

To clarify the statements made immediately above, we perform numerical studies of different closed-dot systems, and compare their resulting eigenfunctions with the wavefunction of their open counterparts [31]. The open system that we study is a hard-walled, stadium-shaped, dot, whose leads are positioned at opposite ends of the stadium (figures 7(*e*)–(*h*)). (The choice of this particular geometry is not critical to our conclusions. We have also performed calculations using self-consistently obtained dot profiles [32].) To study the connection of transport through the open dot to the eigenstates of its equivalent closed system, we calculate the eigenstates and eigenfunctions of the two closed dot shown in figures 7(*a*) and (*b*). The shape of the latter dot is perturbed by including a portion of the connecting leads in its geometry, and in the following, we make use of the ratio of the lead width (w) to the stadium height (h). In figures 7(*c*) and (*d*), we show eigenstates 128–136, and 134–142, of the standard, and perturbed, stadium, respectively. The energy range is roughly the same in these figures and the eigenstates were computed by solving a two-dimensional finite-difference Schrödinger equation with Dirichlet boundary conditions. In figures 7(*e*)–(*h*), we show the results of calculations of the open dot under a number of different conditions (the calculations are for the case of zero temperature, and

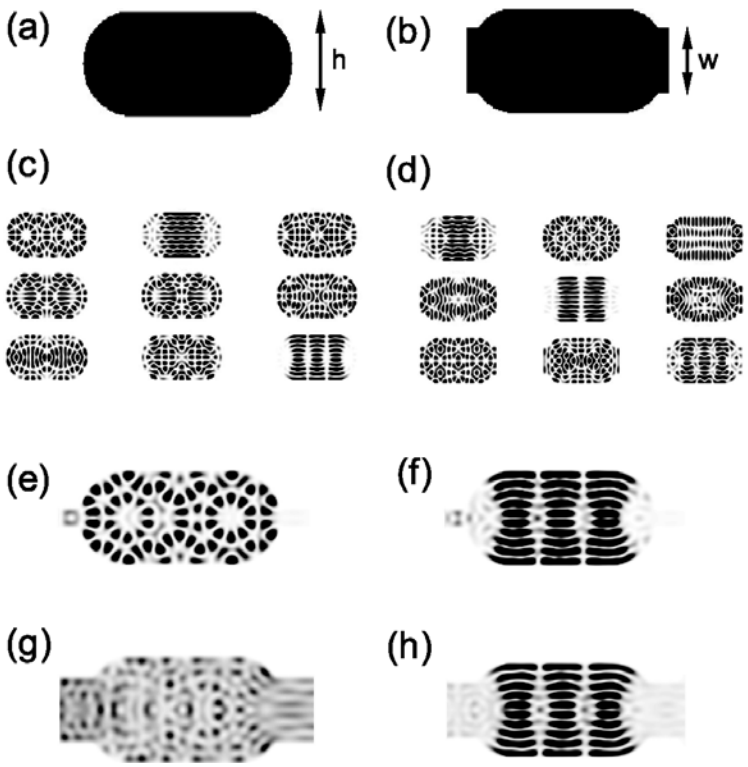

Figure 7. (*a*) Unperturbed stadium. (*b*) Perturbed stadium. (*c*) $|\Psi(x, y)|^2$ vs x and y for eigenstates 128 (top-left) through 136 (bottom-right) of the unperturbed stadium. (*d*) $|\Psi(x, y)|^2$ vs x and y for eigenstates 134 (top-left) through 142 (bottom-right) of the perturbed stadium. (*e*) $|\Psi(x, y)|^2$ for an open stadium with two modes passing through the leads at the energy of the 128th unperturbed-stadium eigenstate. (*f*) As in (*e*), but now the energy is set to that of the 136th eigenstate. (*g*) As in (*e*), but with leads supporting 6 modes. (*h*) As in (*f*), but with 6 modes. Figure reproduced with permission from [31]. Copyright, American Institute of Physics (2002).

were obtained from a numerically stabilized variant of the scattering-matrix approach [33]). In figure 7(*e*), the dot leads support two sub-bands and the energy has been chosen to be equal to that of the 128th eigenstate of the unperturbed stadium. In this case, the wavefunction of the open dot corresponds almost exactly to the isolated-dot eigenfunction (the latter of which is shown at top-left corner of figure 7(*c*)). Figure 7(*g*) is obtained at the same energy as figure 7(*e*), except that now the leads have been opened further to support six modes. In this case, it is clear that any correspondence between the wavefunctions of the open and closed systems has been lost completely. In marked contrast with this behaviour, figures 7(*f*) and (*h*) show that the 136th state of the unperturbed stadium (figure 7(*c*), bottom-right corner) survives, even when the dot leads are opened to support six sub-bands. From these results, it is therefore clear that the different eigenstates of the initially isolated dot develop a highly non-uniform (i.e. state-dependent) broadening when the dot is opened to the reservoirs.

In figure 8(*a*), we show the variation of the open-dot conductance (G) with energy (E, normalized to the average level spacing of the dot, $\Delta = 2\pi\hbar^2/m^*A_\mathrm{d}$, where A_d is the dot area). The squares in the figure indicate the position of the eigenstates of the unperturbed

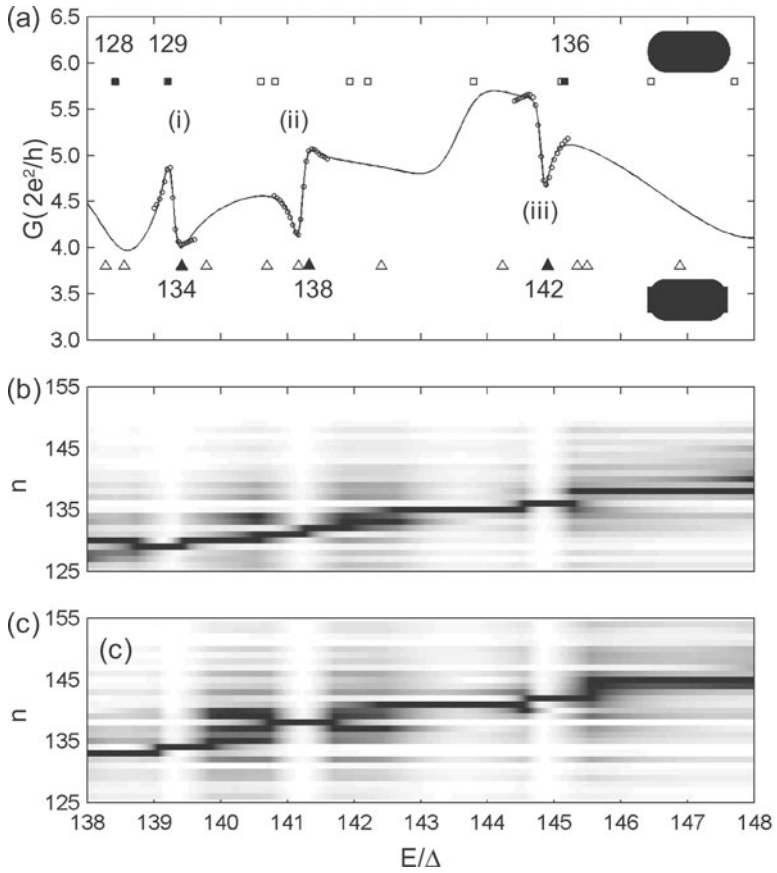

Figure 8. (*a*) $G(E)$ vs E/Δ for the six-mode open stadium ($w/h = 0.6$). Squares and triangles represent the energies of the eigenstates of the unperturbed and perturbed stadium, respectively. (*b*) The normalized decomposition of the open-dot wavefunctions into the unperturbed-stadium eigenstates. (*c*) As in (*b*), but using the perturbed-stadium eigenstates. Figure reproduced with permission from [31]. Copyright, American Institute of Physics (2002).

stadium and we see that eleven such eigenvalues lie in the plotted energy range. In contrast, the conductance shows just three resonances, and the asymmetric lineshape of these features is typical of Fano resonances [34, 35]. Since the closed-dot eigenstates form an orthogonal basis set, the open-dot wavefunction can be expressed as a linear combination of these states:

$$\psi = \sum_n c_n \phi_n^{\text{closed}}, \qquad c_n = \langle \psi | \phi_n^{\text{closed}} \rangle. \tag{2}$$

In figure 8(*b*), the decomposition of the open-dot wavefunctions is plotted as a function of the unperturbed-stadium eigenstate number (n), and E/Δ. The greyscale corresponds to $|c_n|^2/|c_n|^2_{\text{max}}$, so that the peak value of each decomposition is normalized to unity. While for much of the range shown, the open-dot wavefunctions involve a mixture of states, at the energies where resonances (i) and (iii) occur the decompositions are dominated by just a single eigenstate ($n = 129$ and 136, respectively). In contrast, the conductance resonance labelled (ii) corresponds to a mixture of at least two states. Moreover, none of the unperturbed-stadium eigenvalues appear to line up with the position of this resonance. However, a logical assumption is that the leads provide a perturbation to the stadium. We have therefore also computed the eigenstates of the perturbed stadium, which are represented by triangles in figure 8(*a*). It is clear from this figure that the 138th level of this structure coincides with the position of resonance (ii). The decomposition in terms of the perturbed-stadium basis set is shown in figure 8(*c*), where we see that all three conductance resonances are dominated by the contribution of single eigenstates. Referring back to figures 7(*c*) and (*d*), we see that states 134 and 142 of the perturbed stadium bear a strong resemblance to states 129 and 136 of the unperturbed stadium, and occur at similar energies. State 138 of the perturbed stadium, which coincides with resonance (ii) and which closely resembles the open-dot wavefunction at this energy, has no ideal-stadium analogue in the energy range we have considered, however.

In figure 9, we show the decomposition in terms of the perturbed stadium, this time without normalization, however. The positions of the three resonant states are indicated, and it is evident that these states dominate the contribution, relative to all other states. On the eigenvalue axis, we have plotted the eigenenergies of the perturbed stadium relative to Δ, so that the spacing of successive levels is indicated on this axis. Significantly, we see that the width of the 134th state, as inferred from the breadth of the decomposition peak, is larger than the spacing between the 134th and 135th levels, and similar observations may be made for the other resonant states. Nonetheless, the decompositions remain dominated by the contribution of single eigenstates, indicating that the mere proximity of other levels in energy need not be an obstacle to resolving individual states. In fact, as shown in figure 10(*a*), even after performing the summation $\sum_n |c_n|^2$ over a total of 175 states, the contributions from states 134, 138 and 142 still dominate, being a factor of three above the background from all other states. This summation essentially represents the density of states of the open dot. To demonstrate the stability of these states, in figure 10(*b*), we plot $\sum_n |c_n|^2$ vs E/Δ and w/h. As indicated by the shading, the peaks persist over a wide range of lead opening. Also apparent in this plot are peak contours that survive over only a much shorter range of w, before shifting dramatically to lower energy and disappearing.

A critical conclusion that can be drawn from the discussion above is that a highly non-uniform broadening of the eigenstates arises when a dot is opened to its reservoirs. While for the majority of eigenstates the magnitude of this broadening exceeds the average level spacing, a smaller subset of states are only weakly perturbed by the coupling. In the section that follows, we consider the measurable transport results associated with this non-uniform broadening.

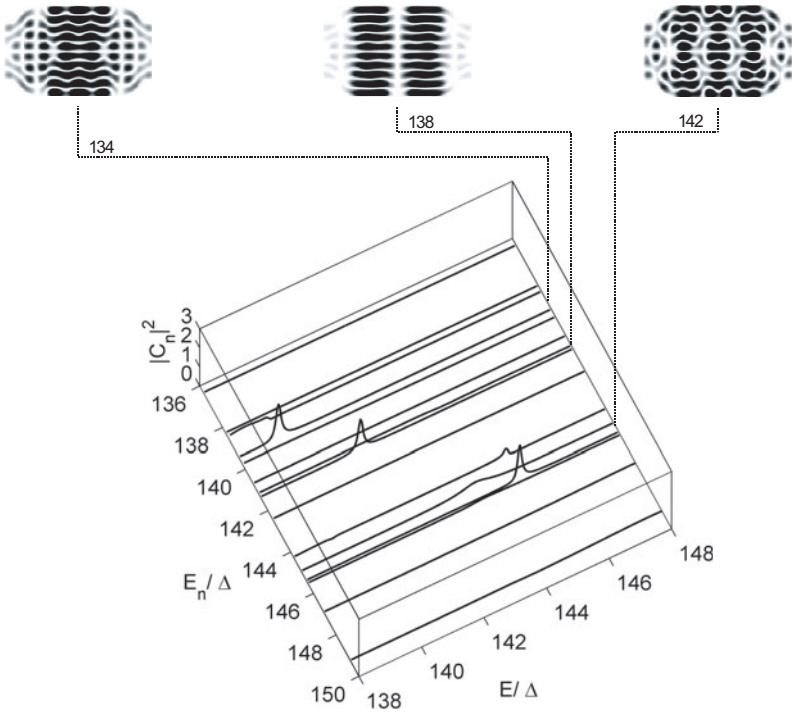

Figure 9. The perturbed-stadium decomposition coefficients $|c_n|^2$ vs E/Δ and E_n/Δ. Figure reproduced with permission from [31]. Copyright, American Institute of Physics (2002).

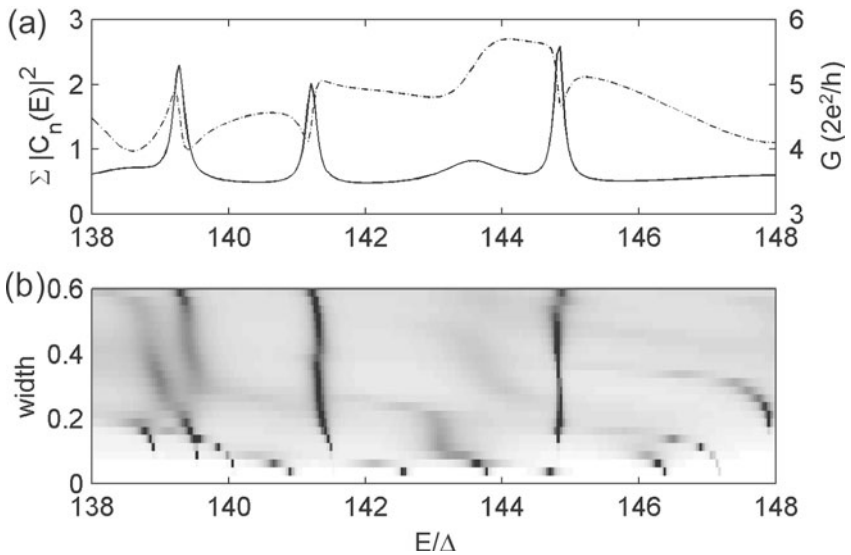

Figure 10. (*a*) $\sum_n |c_n|^2$ vs E/Δ (——, left scale) and $G(E)$ vs E/Δ (- - - -, right scale) for the six-mode open stadium. (*b*) $\sum_n |c_n|^2$ indicated by the shading as a function of E/Δ and fractional lead width, w/h. Figure reproduced with permission from [31]. Copyright, American Institute of Physics (2002).

3.2. Experimental signatures of the open-dot spectrum

While we have thus far considered the case where an energy variation is used to probe the density of states of open quantum dots, in experiment it is more typical to investigate how their conductance varies with magnetic field or gate voltage (figures 3–6). In this section, however, we demonstrate that the effect of these variations is essentially equivalent to sweeping energy, since either the magnetic field or the gate voltage may be used to drive the density of states past the Fermi level, thereby modulating the conductance. To illustrate this point, in figure 11(*a*), we show the computed energy spectrum of a hard-walled, square dot [36]. In figure 11(*b*), we show the numerically calculated magneto-conductance contour for the dot, in the case where current flow through it can occur by means of tunnel barriers that extend uniformly across its width. The greyscale in this figure shows the computed variation of dot conductance with magnetic field and energy [37], and, as one would expect in a resonant-tunnelling problem such as this, we see a clear correlation between points of high conductance in figure 11(*b*) and the discrete states in figure 11(*a*). There is a non-uniform amplitude variation among the different tunnelling resonances, indicating that, even with the coupling provided by uniform tunnel barriers, the influence of this coupling is different for different dot states. In figure 11(*c*), we show the conductance contour obtained in the case where the dot leads have been opened to support four sub-bands. Instead of the simple conductance peaks observed for the tunnelling case (figure 11(*b*)), the resonances found with the leads present tend to exhibit a Fano-lineshape [34, 35], in which resonant transmission peaks are closely paired with resonant minima (not shown). Furthermore, while the conductance of the isolated dot is strongly suppressed in situations where resonant tunnelling is not possible, the open dot exhibits more complicated behaviour. To illustrate this, in figure 11, we have drawn dotted lines at two strategically chosen values of the Fermi energy. The upper line coincides with an energy for which the level spectrum is highly degenerate at zero field. In correspondence with this, the tunnelling transport shows a resonant conductance peak. In figure 11(*c*), however, the zero-field conductance actually shows a minimum at this energy. The second dashed line in

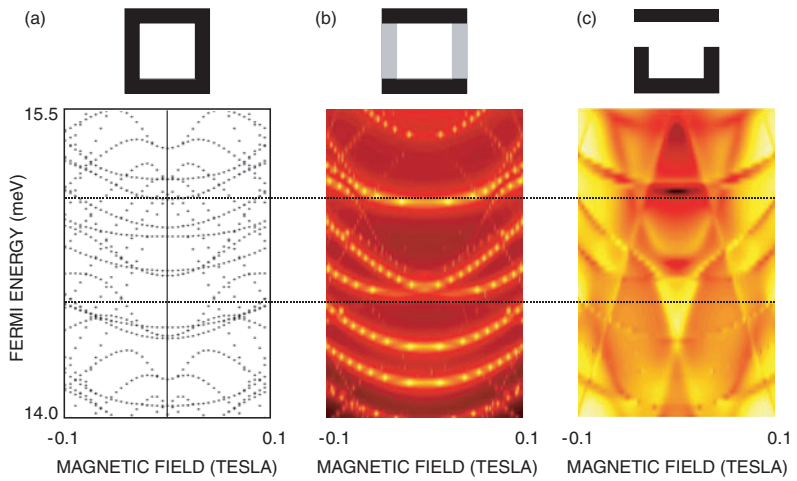

Figure 11. (*a*) The computed energy levels of a 0.3 μm hard-walled quantum dot of square geometry. (*b*) The tunnelling spectrum for the same dot. (*c*) The conductance contour for the dot when its leads are opened to support four propagating modes. In figures 1(*b*)–(*d*), conductance is plotted on a logarithmic scale and brighter regions correspond to points of higher conductance. All calculations were performed assuming a temperature of absolute zero.

figure 11 is positioned at an energy for which no states exist at zero magnetic field, consistent with which tunnelling through the isolated dot is strongly suppressed. In the open dot, however, these maxima are seen to be broadened out sufficiently so that a region of high conductance is actually obtained (figure 11(*c*)).

While the results of figure 11 were computed under the assumption of zero temperature, real experiments are performed at non-zero temperature, where energy averaging arises from thermal smearing of reservoir states and electron dephasing in the dot (the latter of which effects will be discussed in further detail in section 4). To simulate the effect of this averaging on the transport measurements, we adopt the following approach. We first account for thermal smearing and dephasing by introducing an effective temperature (T^*), whose choice is determined empirically by comparison with experiment. The energy-averaged magneto-conductance may then be computed from a simple convolution of the zero-temperature conductance with the derivative of the Fermi function:

$$G_{\mathrm{av}}(B, E_{\mathrm{F}}, T) = \int G(B, E) \left[-\frac{\mathrm{d}f(E - E_{\mathrm{F}}, T)}{\mathrm{d}E} \right] \mathrm{d}E, \tag{3}$$

where E_{F} is the Fermi energy. For a demonstration of these concepts, in figure 12 we show the evolution of the magneto–resistance of another quantum dot with gate voltage. To realistically model the transport through this dot, we calculate its profile self-consistently, and compute its energy-averaged magneto-conductance at several different values of E_{F}. A comparison of the calculations with selected experimental curves is provided in figure 13, where we have assumed that $T^* = 0.3$ K, which appears to provide the best agreement with the results of experiment. It is clear from these figures that our simulations are successful in reproducing the main features of experiment. The discrepancy between the value of T^*, and the cryostat temperature of 0.01 K, cannot be attributed to an inability to cool the electrons in the dot below 0.3 K. Later on in this review, we will discuss the observation of temperature-dependent resistance variations in these dots, which exhibit a consistent change at temperatures well below

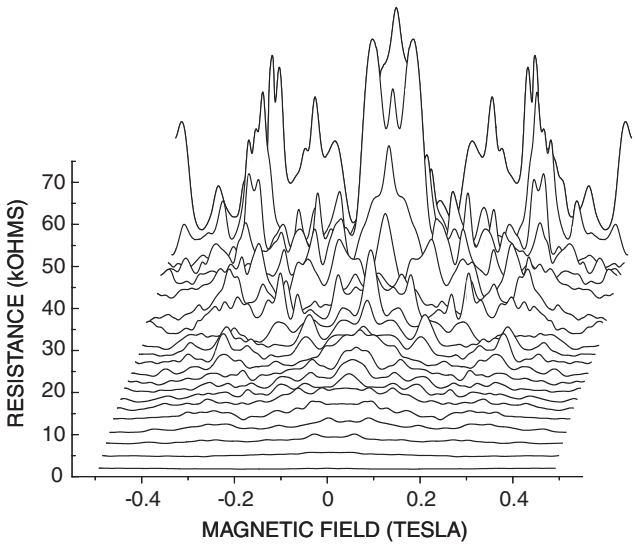

Figure 12. The measured variation of the low temperature (0.01 K) magneto–resistance of the 0.4 μm quantum dot with gate voltage. These magneto–resistance measurements were taken at twenty two unequally spaced gate voltages ranging from −0.3610 to −0.4335 V. Figure reproduced with permission from [36]. Copyright, American Physical Society (1999).

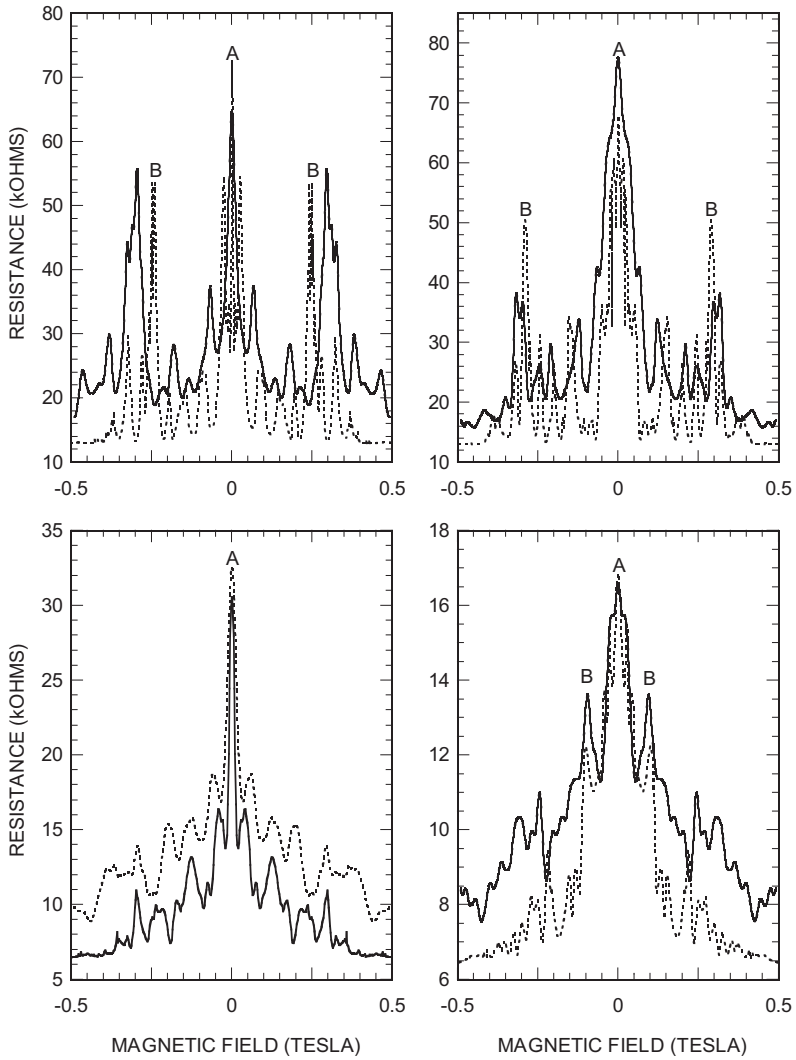

Figure 13. Selected magneto–resistance curves from figure 12 (——) are compared with the results of simulations (- - - -). Upper left (experiment): $V_g = -0.4295$ V. Upper left (simulation): $V_g = -1.05$ V, $E_F = 15.75$ meV. Upper right (experiment): $V_g = -0.4260$ V. Upper right (simulation): $V_g = -1.05$ V, $E_F = 16.1$ meV. Lower left (experiment): $V_g = -0.4000$ V. Lower left (simulation): $V_g = -0.922$ V, $E_F = 15.1$ meV. Lower right (experiment): $V_g = -0.3885$ V. Lower right (simulation): $V_g = -0.922$ V, $E_F = 15.5$ meV. Figure reproduced with permission from [36]. Copyright, American Physical Society (1999).

0.05 K [38–40]. Another contribution to T^* is from decoherence-induced broadening of the dot levels, and the magnitude of this effect is determined by the value of the phase-breaking time (τ_ϕ). Essentially, this can be thought of as the average time over which the electron is able to propagate within the dot, before its wave coherence is destroyed by scattering events [27]. With a conservative estimate of 100 ps for this timescale (see section 4), however, we infer a corresponding level broadening ($\hbar/k_B\tau_\phi$) of roughly 0.1 K. It therefore seems that an additional source (or sources) of broadening contributes to the determination of T^*. The source of this

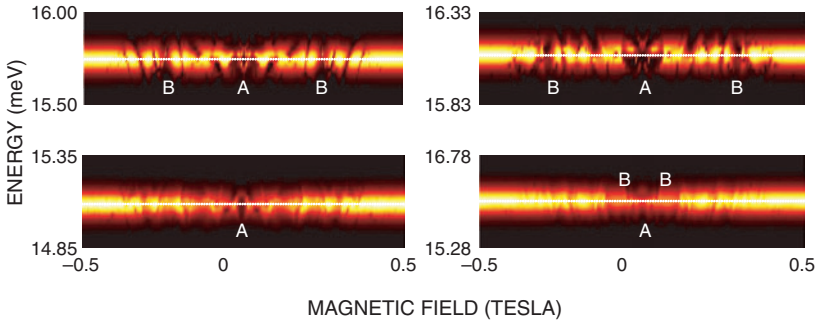

Figure 14. The conductance is convoluted with the derivative of the Fermi function and then plotted as a function of energy. The four figures correspond, in the same sequence, to the computed magneto–resistance plots shown in figure 13, while the symbols *A* and *B* denote the major magneto–resistance features seen in figure 13. Figure reproduced with permission from [36]. Copyright, American Physical Society (1999).

additional broadening remains unclear, although it may be associated with the influence of disorder-induced electron scattering in the dot [41].

While the discussion above serves to demonstrate the ability of realistic modelling to capture the key details of quantum-dot transport, we have not yet made clear the nature of the connection between the conductance curves in figures 3–6 and the density of states of the open dot. As we have mentioned, the basic idea is that the magnetic field or gate voltage may be used to sweep discrete dot states past the Fermi level, giving rise to an associated modulation of the conductance. The number of discrete dot states that contribute to the conductance at any magnetic field is therefore determined by the details of the density of states, and the width of the energy window over which energy averaging is effective. At the low temperatures of interest here, the size of this window is relatively narrow and the magneto–resistance can exhibit features associated with the movement of specific dot eigenstates past the Fermi level. To illustrate these notions, we show in figure 14 the conductance contours that were used to calculate the magneto–resistance curves in figure 13. The contours were obtained by convolving the magneto-conductance with the derivative of the Fermi function at a number of different energies. Bright regions in the contours correspond to high conductance and, at the low temperatures of interest here, only a narrow window contributes effectively to the energy average. An important feature of the contours is the series of bright and dark lines that pass through the Fermi level at different magnetic fields. In figure 11, we saw that these lines trace the evolution of the density of states as magnetic field and Fermi energy are varied. It is the presence of these lines that sets the position and widths of the major magneto–resistance peaks seen in experiment and theory. The width of the central peak found in the lower left panel of figure 13 (marked A), for example, is set by a pair of resonance lines that bound the local conductance minimum in the centre of the lower left panel of figure 14. Examining the other panels in figure 14, it is evident that similar features limit the width of the central peak in all other cases depicted in figure 13. Similarly, the side-peaks seen in the upper two plots of figure 13 result from the presence of a low conductance region that is bounded by resonances which cross the Fermi level near $\pm 0.3\,\mathrm{T}$ (figure 14, upper two panels). Interestingly, the side-peaks are seen to be strongest in situations where the dot leads are configured to support just a few modes, a property that is apparent in both experiment and theory. The side-peaks might be mistaken as arising from a classical magneto-focusing effect, in which the curvature of electron motion induced by the magnetic field focuses electrons into the input or output

leads, at magnetic fields where the cyclotron radius is commensurate with the size of the dot. Such an effect can be ruled out here, however. First, we note that the magnetic field values at which the peaks occur do not correspond to any obvious commensurability condition in the dot. Second, the peaks wash out rapidly with increasing temperature (not shown here), while focusing-related features are known to persist to very much higher temperatures [42–45].

The influence on the conductance of the eigenstates of the open dot, as they cross the Fermi level as the magnetic field is varied, is shown more clearly in figure 15. The upper panel of this figure shows the computed conductance contour of an open dot and, in the middle panel of figure 15, this contour is convoluted with the derivative of the Fermi function, to show

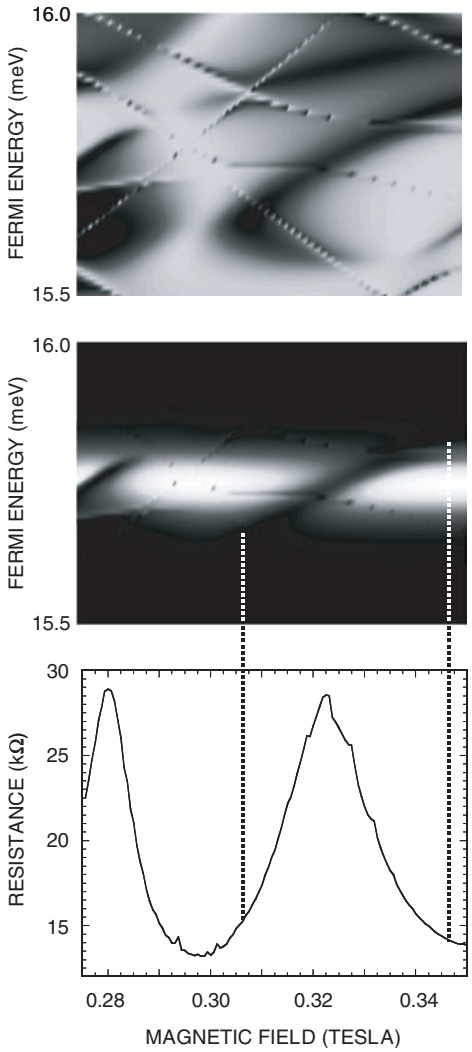

Figure 15. Top: computed conductance contour of a 0.4 μm dot. Middle: the contour obtained after convolving the conductance with the derivative of the Fermi function, assuming an effective temperature of $T^* = 0.3$ K. Bottom: the energy-averaged magneto-conductance of the dot, computed assuming an effective temperature of $T^* = 0.3$ K. Figure reproduced with permission from [36]. Copyright, American Physical Society (1999).

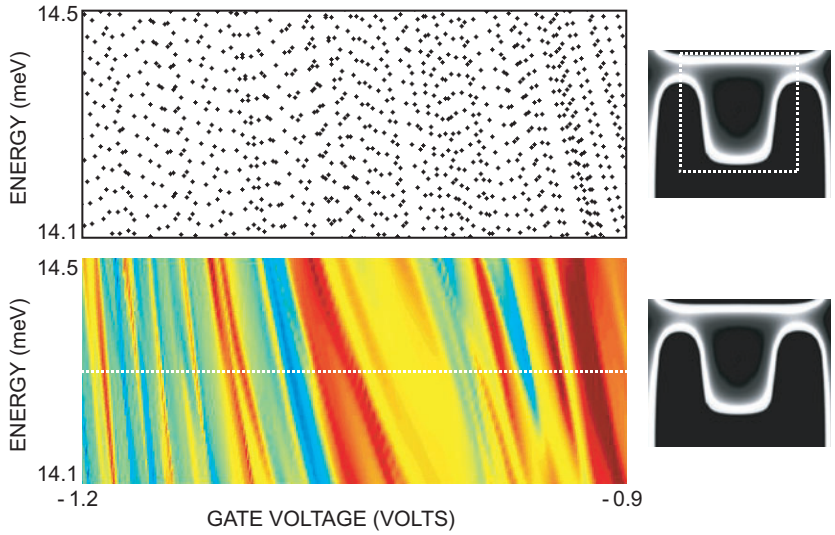

Figure 16. Upper plot: evolution of the closed-dot eigenstates with gate voltage for a dot of size 0.4 μm. Lower plot: computed variation conductance with gate voltage and energy for the same dot. The greyscale varies from 0 to $2e^2/h$ and the dashed line shows the Fermi energy. Figure reproduced with permission from [32]. Copyright, American Physical Society (1999).

the range of energies that effectively contribute to the conductance. Here, we focus on the dark striation that passes through the Fermi level over the magnetic field range between 0.3 and 0.35 T. This striation represents the passage of a broad resonance past the Fermi level and it is easily seen that the magnetic field range over which the crossing occurs determines the effective width of the resulting resistance peak.

While the discussion above focuses on the use of a magnetic field to probe the density of states of the open dots, we have also mentioned that a gate-voltage variation may be used to achieve essentially the same effect [32]. This idea is illustrated in figure 16, in the upper panel of which we show the computed variation of the energy levels of an isolated dot with gate voltage. In these calculations, the variation of the quantum-dot profile with gate voltage is computed self-consistently, and the energy levels of the closed system are obtained by artificially closing the leads at their narrowest points (see figure 16). As the gate voltage is made progressively negative, the levels shift upwards in energy, which is a direct consequence of the gate-voltage induced decrease in the size of the dot (see figure 2). In the lower panel of figure 16, we show the contour plot obtained by computing the variation of the conductance of the equivalent open dot with gate voltage. Similar to our discussion of the magneto-conductance contours (figure 11), distinct lines can be seen running through this plot, and which clearly follow the motion of certain closed-dot states. Not all states give rise to a marked modulation of the conductance, however, and this is nothing more than a consequence of the non-uniform level broadening that we have shown to arise in the quantum-dot spectrum when the leads are opened to the reservoirs. In experiment, of course, the variation of conductance with gate voltage is measured at fixed Fermi energy, as indicated by the dotted line in the lower panel. As the gate voltage is used to drive successive dot states past this reference energy, oscillations are observed in the conductance (figure 6). Similar to our discussion of figures 14 and 15, the lineshape of these oscillations is determined by the coupling-induced broadening of the original dot states, and the range over which energy averaging is effective (i.e. temperature

and dephasing). In this sense, we see that the conductance fluctuations observed in figure 6 may be viewed as arising from essentially the same phenomenon as those in figures 3–5.

3.3. Wavefunction scarring in open quantum dots

The central result of sections 3.1 and 3.2 is that the discrete states of an isolated dot are broadened non-uniformly when its leads are opened to the reservoirs. For certain states, this broadening can be much smaller than the average level spacing, allowing them to give rise to directly measurable transport results. While we have provided detailed numerical calculations, and experimental data, to support these arguments, we have not yet considered explicitly the origin of the non-uniform broadening. This is easy to understand, however, if we consider the behaviour shown in figures 7 and 9. Close inspection of these figures reveals that the strongest correspondence between the closed- and open-dot wavefunction arises when the latter show a large buildup of probability density in regions located away from the leads. In other words, the robust states of these systems are those that couple only weakly to the leads, a result which seems quite intuitive.

An interesting feature of those states that remain resolved in the open dot is that their wavefunctions tend to be scarred [46, 14] by the remnants of a small number of semiclassical orbits. The characteristic signature of the scarring is a buildup of probability density in the dot, which is organized along the path of particular classical orbits. This property can be seen in the wavefunctions of figures 7(f) and (h), which show the signature of a trapped orbit that bounces back and forth between the parallel faces of the dot. Since this mode couples only weakly to the leads, it is able to remain resolved in the open dot, even when its leads are opened to support many occupied sub-bands (figure 7(h)). An important feature of the scars, and one which we have demonstrated to have measurable transport results, is that they regularly recur as the magnetic field or gate voltage is varied [32, 47–50]. This property is illustrated in figure 17, which shows the results of calculations of the wavefunction of a realistic quantum dot, at a series of different gate voltages. These plots were obtained by first of all calculating self-consistently the potential profile of the dot, at each of the fifty gate voltages shown in figure 17 [51, 52]. Using these profiles, the probability density in the dot was then determined at each gate voltage. In most of the cases shown in figure 17, the probability density exhibits an essentially random form, which rapidly evolves as the gate voltage is varied. In certain cases, however, the wavefunction is scarred by what appear to be whispering-gallery (W) and bouncing-ball orbits (B). When the gate voltage is varied over a much wider range than shown in figure 17, the scars recur periodically as we illustrate in figure 18. The upper two rows of this figure show the set of whispering-gallery scars, which recur at a frequency of 38 V^{-1} for this dot, while the bottom two rows show variants of bouncing-ball scars. Both sets of these scars recur at a frequency of 15 V^{-1}, but are phase-shifted from each other by a fixed increment of 20 mV.

In figure 19, we show the computed magneto–resistance of a square dot at 0 K [48]. As the magnetic field is varied, the resistance exhibits many resonances and, at the magnetic fields indicated by the dotted lines, these are seen to be related to the presence of a diamond-like wavefunction scar. The scar recurs with an almost constant magnetic-field period of 0.11 T, and the resonances in the conductance provide a measurable transport result associated with this recurrence. Of course, the calculations in figure 19 are performed for the case of zero temperature, and it is not immediately obvious that the transport signatures of the wavefunction scars should remain observable under typical experimental conditions. For this reason, in figure 20, we show a more realistic manifestation of the scarring behaviour. The dot studied here is the same as that considered in figures 17 and 18, in which the gate voltage

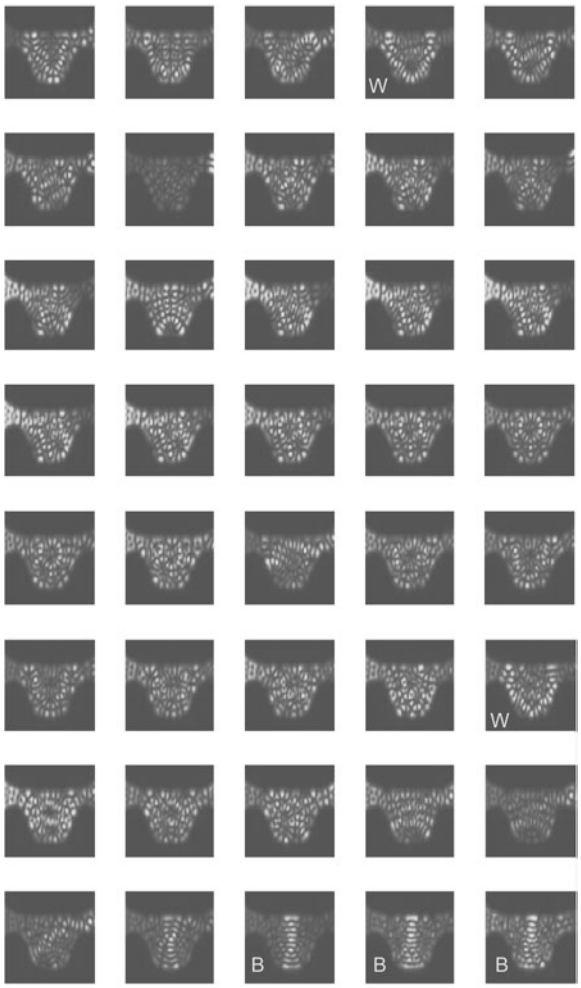

Figure 17. The calculated variation of the probability density as a function of gate voltage, for the dot considered in figure 16. From top-left to bottom-right the gate voltage is stepped in 1 mV increments between −0.900 and −0.851 V. Lighter regions correspond to higher probability density.

is varied to induce a modulation of the scarring patterns. In the upper inset to figure 20, we show the measured conductance oscillations for the gate-voltage variation. The oscillations were obtained by subtracting a slowly varying background (see, e.g. figure 6) from the overall conductance variation induced by the gate voltage [32]. Also shown in the same inset, are the numerically computed conductance oscillations. The calculations are performed for a gate voltage-dependent, self-consistent, dot profile, and properly account for the influence of finite temperature and dephasing [37, 48]. From a comparison of the two curves in the inset, it is clear the frequency content of the experimental oscillations is well reproduced by the calculations. This is confirmed in the main panel of figure 20, where we plot the Fourier spectra of both sets of oscillations. The spectra exhibit a number of well-defined peaks, the largest of which occurs at a frequency of $15\,\mathrm{V}^{-1}$. As we have discussed, this corresponds closely to the frequency with which the two types of bouncing-ball scars (denoted by '1' and '2' in figure 20) recur with gate voltage. We have mentioned already that these two

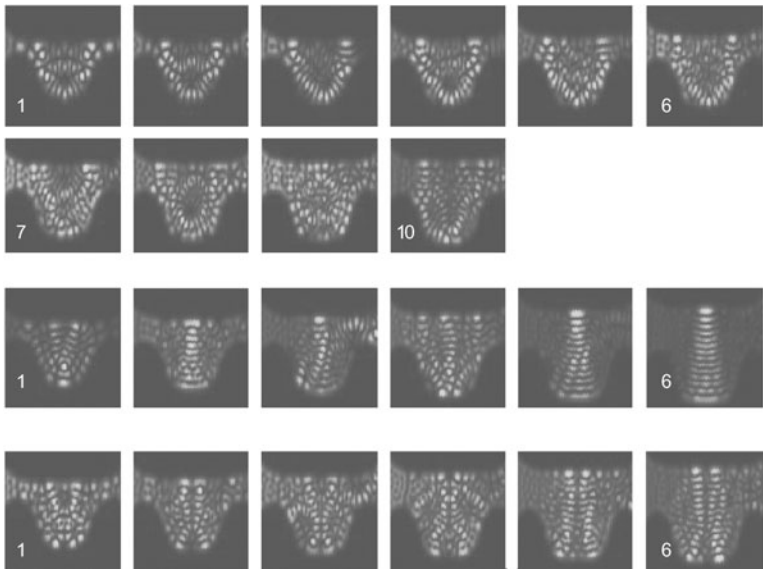

Figure 18. Recurring scars in the dot geometry of figure 16. Top two rows are whispering-gallery scars. For each of the three scar types, moving from left to right corresponds to moving to less-negative gate voltage.

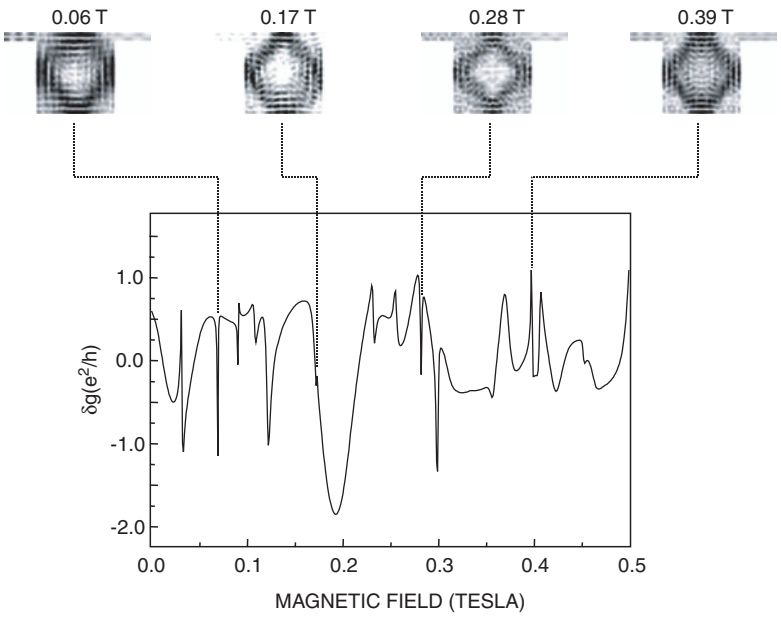

Figure 19. Recurring wavefunction scars and the magneto–resistance of a square-shaped quantum dot. The calculations are performed for a temperature of 0 K, using the method described in [48].

scars are shifted from each other by a fixed increment of 20 mV, and this appears to account for the common peak at 50 V^{-1} in both spectra. The other major peak in this figure occurs at 38 V^{-1}, in good agreement with the recurrence properties of the whispering-gallery scar, shown in the upper two rows of figure 18. Based on these observations (figures 18–20), we

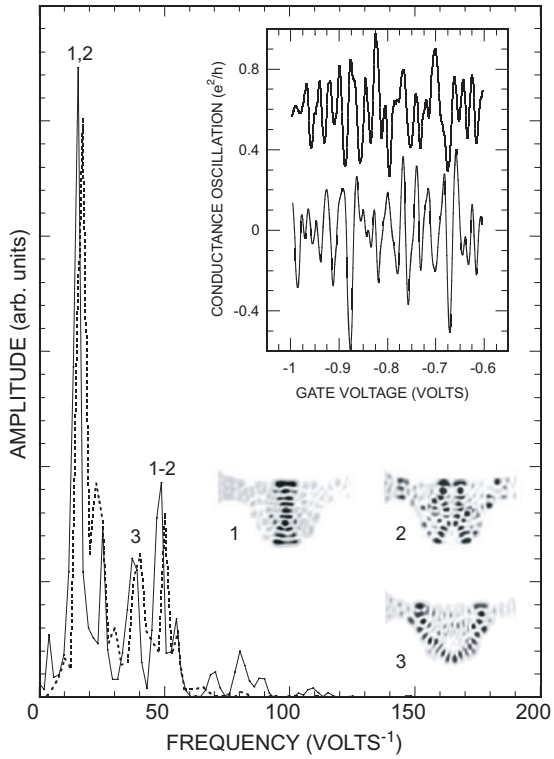

Figure 20. The upper curve in the inset shows the conductance oscillations generated in a dot of size $0.4\,\mu$m as a function of gate voltage (a slowly varying background has been subtracted from the overall conductance oscillation), while the lower curve shows the results of numerical calculations. (The upper curve is offset by $+0.6e^2/h$.) The main panel shows the Fourier spectra of measured and computed oscillations (- - - - is theory). Lower inset: recurring scars of this dot. The numbers here show the association between specific scars and Fourier peaks and dark regions correspond to high probability. Figure adapted from [32]. Copyright, American Physical Society (1999).

conclude that measurable transport results associated with the scars can indeed be observed in experiment.

To summarize the main results of this section, we have seen that the robust states of open dots, that survive in the presence of strong coupling to the environment, correspond to those eigenstates of the closed system that are scarred by periodic orbits, which buildup probability density away from the leads. The scars recur periodically as the magnetic field or gate voltage is varied, and appear to give rise to associated transport results [32, 49, 50] (figures 4, 6 and 20). In the following section, we consider how the scars may be accounted for within a semiclassical perspective. This discussion will show that the scars are consistent with the process of dynamical tunnelling, in which electrons tunnel through isolated regions of phase space, into classically inaccessible orbits.

3.4. Dynamical tunnelling and the semiclassical description of open quantum dots

In a semiclassical description of transport in the dots, the objective is to describe their electrical characteristics by considering the interference of electron partial waves that propagate through

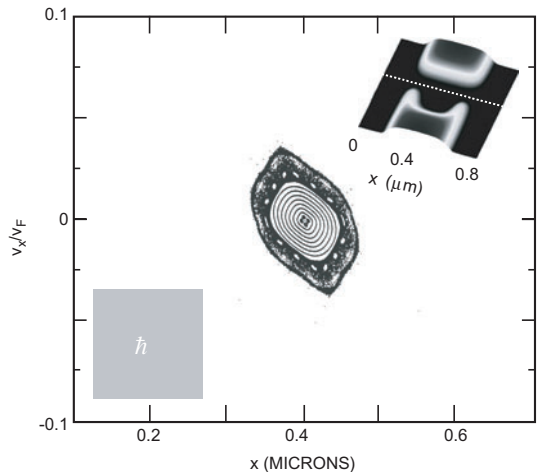

Figure 21. Poincaré section of motion calculated for the open quantum dot of figure 20. The section is taken along the dotted line in the upper inset. The lower inset shows an area of phase space comparable in size to $\hbar$.

the dot along different classical paths [53]. The starting point for such an analysis is the classical phase space for electron motion in the dot, and in many studies in the literature it is often typically assumed that this dynamics is fully hyperbolic (fully chaotic). In this situation, all orbits are unstable and all initial conditions escape from the dot in a finite time (except for a set of null measure). The Poincaré section of motion in this case should therefore correspond to a dense set of points, with no evidence for any stable orbits. As we show in figure 21, however, the actual section of motion of these dots typically exhibits a mixed nature, with clear evidence for the presence of Kolmogorov–Arnold–Moser (KAM) islands [54]. The nonhyperbolic nature of the dynamics appears to be a quite generic property of these dots [55–58]. The KAM island in figure 21 is centred on a period-one orbit that bounces back and forth at the centre of the dot, just as we saw earlier in our discussion of wavefunction scarring in this structure (figures 17, 18 and 20). A crucial point to note, however, is that orbits such as this, within the KAM island, are classically inaccessible to electrons injected into the dot by its connecting leads.

The standard approach for relating the conductance of quantum dots to their classical dynamics, involves expressing the quantum-mechanical transmission probability of the dot in terms of a uniform sum over all trajectories that connect the input and output leads [53]. This approach therefore neglects any contribution to transport from isolated orbits, contained within KAM islands. In systems whose size is comparable to the de-Broglie wavelength (λ_F), however, it is now understood that the process of dynamical tunnelling can occur, in which the particle involved tunnels through the classically forbidden regions of phase space to access isolated orbits [59–62]. While experimental demonstrations of this effect have recently been provided in microwave cavities [63], and in cold-atom systems [64, 65], its role in transport in mesoscopic structures has not been widely considered. For dots with a typical size of a micron or less, we have seen that λ_F is typically within an order of magnitude of the dot size, and we have therefore argued that the tunnelling effect cannot be neglected in such structures [54].

Since KAM separatrices are classically impenetrable, the classical dynamics within them may be viewed as that of a closed system. Because of the dynamical tunnelling, however, there is a probability that an incoming electron may tunnel onto the KAM island, when its energy

and the system parameters are such that the semiclassical quantization condition is satisfied for a low-period stable orbit within the island. For a closed system, it is well known from the expansion of the Gutzwiller trace formula that each stable orbit generates a series of delta functions in the density of states, corresponding to energies for which the following resonance condition holds [66]:

$$S_{\mathrm{eff}} = S + \frac{\omega}{2\pi}\left[m + \frac{1}{2}\right] + \frac{\lambda}{4\pi}, \qquad m, n = 0, 1, 2, \ldots. \tag{4}$$

In this expression, S_{eff} is the effective action of the orbit, ω is its stability angle, and λ is the Maslov index. S is the action along the classical orbit in units of the Planck constant:

$$S = \int \frac{1}{h}\boldsymbol{p}\,\mathrm{d}\boldsymbol{q}. \tag{5}$$

For a closed system, and for each energy that satisfies equation (4), there is a delta function in the density of states, corresponding to a discrete energy level. Our system is open, however, and just as an incoming electron may tunnel in, an electron within the island may also tunnel out, causing the associated energy level to develop a finite width. If the effective trapping time within the orbit is much longer that required for the electron to undergo one period of motion, however, this broadening may be much smaller than the characteristic energy spacing between the different levels. In this situation, the dynamical tunnelling can be expected to cause a strong modulation of the conductance through the dot.

While it is our opinion that the dynamical tunnelling effect should be quite generic to mesoscopic structures, to provide a clear demonstration of its importance we consider its role in giving rise to the wavefunction scarring, found in figure 20. Consider first the case where $m = 0$. n may be viewed as a longitudinal quantum number, which counts the number of wavefunction nodes along the orbit. For the KAM island shown in figure 21 there are infinitely many periodic orbits, but only the lowest period ones are expected to remain resolved, since the others should give rise to energy levels that are too closely spaced to be resolved. Clearly, the most important orbit in the island is the period-one bouncing-ball orbit, which corresponds to the fixed point at the centre of the KAM island. We calculate S_{eff} in equation (4) numerically, as a function of the gate voltage for this island, and compare to the experimental results [54]. The result is plotted in figure 22, where we see that the points fall on reasonably straight lines, which corresponds to a periodic recurrence of the resonance, and a periodic oscillation in the conductance. Since a conductance resonance should occur each time S_{eff} changes by one, the (absolute value of) the slope of the resulting straight line directly gives the semiclassical prediction for the frequency of the associated conductance oscillations. We find this frequency to be $16.4\,\mathrm{V}^{-1}$, in remarkably good agreement with the measured value of $15\,\mathrm{V}^{-1}$ for the bouncing-ball scar in figure 20. That is, the component of the conductance oscillations at this frequency appears to be related to recurring tunnelling resonances of the bouncing-ball orbit.

Now consider the general case, when m is any positive integer. The second term on the right-hand side of equation (4) represents the quantization of the component of the motion transverse to the periodic orbit. That is, for each value of n, there is actually a set of resonances labelled by m, similar to the vibrational band of a molecule. In figure 16, we saw that the energy levels of the dot shift linearly with gate voltage, at least over the range considered here, and it is this property that gives rise to the linear variation of S_{eff} in figure 22. Assuming such a variation of S_{eff}, we can estimate the gate-voltage separation of two resonances with consecutive transverse quantum numbers:

$$\Delta V_{\mathrm{g}} = \frac{\omega}{2\pi}\left|\frac{\mathrm{d}S_{\mathrm{eff}}}{\mathrm{d}V_{\mathrm{g}}}\right|^{-1}, \tag{6}$$

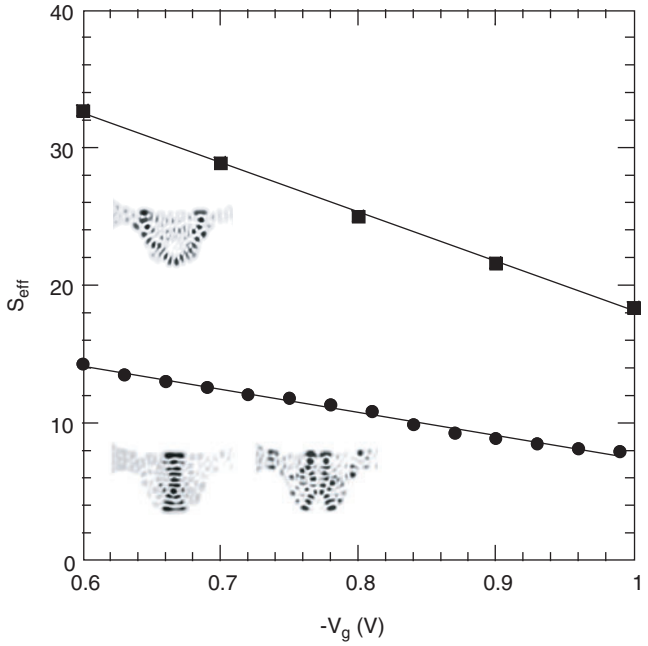

Figure 22. Effective action vs the gate voltage, for the stable (●) and the unstable (■) orbits. The lower inset shows a pair of closely spaced concentrated wavefunctions corresponding to the stable bouncing-ball orbit. The upper inset shows a scar due to the unstable orbit. Figure reproduced with permission from [54]. Copyright, American Physical Society (1999).

where we have assumed that the value of ω does not change much between resonances. This is actually quite reasonable, since, although ω does depend on n, its values are found numerically to lie within the range between 1 and 2 rad. Using the value of $\mathrm{d}S_{\mathrm{eff}}/\mathrm{d}V_{\mathrm{g}}$ determined from figure 22, equation (6) yields a value of ΔV_{g} between 10 and 20 mV. Just as n counts the number of nodes along the orbit, m counts the number of nodes across it, so we expect that for each value of n (corresponding to a fixed number of longitudinal nodes in the eigenfunction), there should be a set of scars having 0, 1, 2, ... transversal nodes, separated by a gate-voltage interval of 10–20 mV. Such behaviour is seen clearly in experiment, where two variants of the bouncing ball occur (labelled '1' and '2' in figure 20), and are shifted from each other by a fixed increment of 20 mV. We stress that this phenomenon cannot be accounted for without invoking the influence of dynamical tunnelling, since it requires that the electrons have access to the stable orbit, which is classically, and also semiclassically, forbidden. Scars corresponding to higher values of m are not observed in the quantum-mechanical calculations, presumably because they have a short life-time. As can be seen in figure 20, the $m = 1$ wavefunction ('2') has a wide lateral extent, which should increase even more as m is increased. For values of $m > 1$, we therefore expect that the wavefunction will have a large overlap with regions of phase space outside of the KAM island, and that the associated resonances will be very short lived.

Although we have thus focused on the signatures of dynamical tunnelling due to stable orbits, unstable orbits are present in the system and may also contribute to the density of states. The resonance condition for unstable periodic orbits is given by equation (4), without the ω term [66], so that these orbits do not give rise to the sub-band of resonances associated with different values of m. The scar corresponding to the main unstable orbit

is the whispering-gallery scar, labelled '3' in figure 20, and which recurs with a frequency of approximately $38\,\mathrm{V}^{-1}$. In figure 22, we plot the variation of S_{eff} with V_{g} for this orbit, and obtain a recurrence frequency of $36\,\mathrm{V}^{-1}$, in very good agreement with the experimental observation.

The main conclusion to be drawn from the discussion above is that usual semiclassical approaches to the description of transport, which consider only the contribution from classically accessible trajectories, are insufficient to explain the observed characteristics of quantum dots. Instead, the quantum-mechanical tunnelling of electrons through KAM islands has to be taken into account. The tunnelling may be mediated by stable, or unstable, periodic orbits, and gives rise to conductance oscillations whose characteristics agree well with the results of experiment. While we have focused on a specific experimental system, to demonstrate the key principles of the tunnelling effect, our results are believed to be of general applicability to mesoscopic systems. Indeed, periodic conductance oscillations, with characteristics similar to those discussed here, have been observed in a number of different experimental studies of open dots [32, 49, 50].

3.5. Open quantum-dot molecules

In the preceding sections, we have focused on the development of consistent quantum-mechanical, and semiclassical, interpretations of the transport properties of open quantum dots. Another interesting question that arises, however, concerns the modifications to the transport properties that arise, when several dots are coupled coherently to each other. It is this problem that we explore in this section, where we investigate the details of electron interference in coupled quantum dots.

In figure 23, we show the magneto–resistance of a split-gate quantum-dot array, at several different values of its gate voltage [67]. The array consists of three identical, series-connected, dots (see the inset to figure 23), and its magneto–resistance is, in many ways, reminiscent of that exhibited by the single dots that we have discussed thus far. In figure 24, we show examples of the magneto-conductance fluctuations exhibited by the array. The measurements shown in the left-hand panel were obtained at six, closely-spaced, values of the gate voltage for which the average conductance of the array was close to $7e^2/h$. In contrast, the right-hand panel was obtained with the conductance close to $3e^2/h$, and a comparison of the two plots reveals a striking difference in the frequency content of their fluctuations. In particular, reducing the average conductance of the array causes a suppression of the high-frequency components of the fluctuations. This evolution can be seen in more quantitative fashion in figure 25, where we use contours to plot the gate-voltage-dependent evolution of the fluctuation Fourier spectra in two different arrays. (These plots were constructed from measurements performed at fifty, equally spaced, gate voltages in each array.) As the gate voltage is made more negative, a damping of the high-frequency features in the contours occurs, consistent with the evolution shown earlier in figure 24.

Since an important effect of the gate-voltage variation is to change the strength of the inter-dot coupling in the arrays, we have argued that the change in the frequency content of the fluctuations, shown in figures 24 and 25, is associated with this change in the coupling strength [67]. We recall here that our investigations of open dots have revealed an intrinsic connection between their conductance and their density of states. Given this connection, the behaviour exhibited in figures 24 and 25 appears to indicate that the level spectrum of the arrays develops a finer structure as the inter-dot coupling is increased, and we believe that this effect results from a coupling-induced hybridization of the density of states in the arrays. Such hybridization behaviour has, in fact, been predicted numerically [68], as we

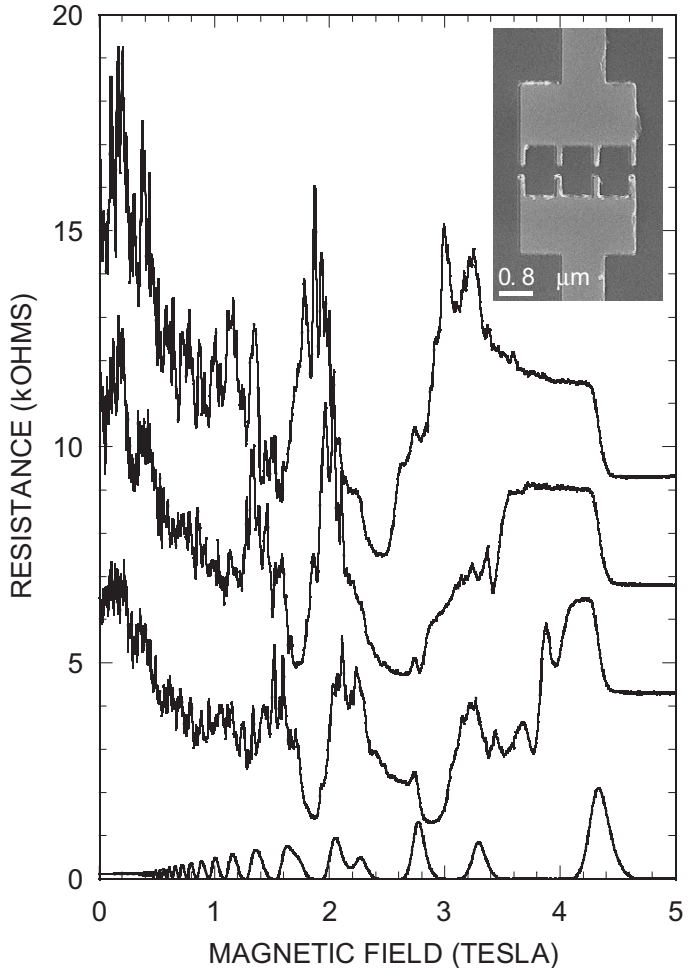

Figure 23. The gate-voltage dependent evolution of the magneto–resistance of a three-dot quantum-dot array with dot dimensions of $0.6 \times 1.0\,\mu\mathrm{m}^2$. The inset shows a scanning electron micrograph of an array with a similar geometry to that studied here. Figure adapted from [67]. Copyright, American Physical Society (2001).

illustrate in figure 26. From left to right in this figure, we compare the computed magneto-conductance contour of a single dot, to the contours obtained in calculations for quantum-dot arrays, consisting of four, and ten, identical dots, respectively. Darker regions in these contours correspond to low conductance, and magnetic field and energy are plotted on the horizontal, and vertical, axes, respectively. As the number of dots in the array is increased, we see from the contours that their features develop increasing fine structure, which directly reflects the formation of superlattice states in the coupled systems [68]. The indication of the experimental work here is that the extent of this hybridization can be sensitively controlled, by using a gate voltage to vary the inter-dot coupling in the arrays. Support for this conclusion has recently been provided by independent experimental work, in which the transport through a system of coupled dots with independently tunable inter-dot coupling strength was investigated [69].

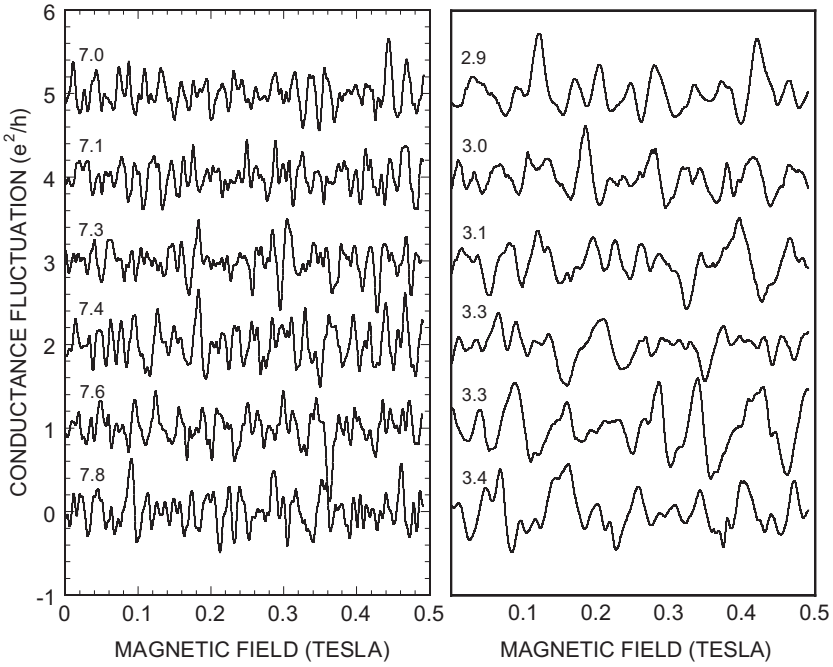

Figure 24. Conductance fluctuations measured in array with dot dimensions of $0.4 \times 0.7\,\mu\mathrm{m}^2$. Successive curves differ by a gate-voltage increment of 10 mV and are shifted upwards by e^2/h for clarity. The average conductance in e^2/h is indicated by the numbers on the left-hand side of each plot. Figure reproduced with permission from [67]. Copyright, American Physical Society (2001).

3.6. Comparison with other studies

3.6.1. Other work on quantum dots. In the preceding sections, we have developed a description of transport in the open dots that may be understood consistently, using either semiclassical or quantum-mechanical concepts. The ability of this description to accurately account for the behaviour observed in experiment may be traced to the fact, that it is founded on a proper treatment of the device-specific aspects of the transport. This should be contrasted with a large number of studies in the literature, which assume a mathematically-convenient, yet physically-artificial, model for the transport. A typical assumption, in particular, is that the classical dynamics in the dots is fully chaotic, and therefore characterized by a single escape rate. The advantage of such an assumption is that it allows the semiclassical expression for the dot conductance to be reduced to a simple analytic form [53]. It also allows one to establish an analytic connection between the properties of the conductance fluctuations and the electron phase-breaking time (τ_ϕ) [70,71]. An important consequence of the single escape rate, associated with the chaotic dynamics, is that one expects the discrete levels of the dot to develop a uniform broadening due to its coupling to the reservoirs [70,71]. Moreover, for the open dots of interest here, the magnitude of this broadening should always be larger than the average level spacing, so that sharp features due to specific eigenstates are not expected to be resolved in the transport. Although mathematically appealing, the problem with these arguments is that they are physically incorrect. As we have seen, opening the dot to its reservoirs gives rise to a highly non-uniform level broadening, allowing certain states of the closed system to remain resolved, and so to give rise to associated features in the conductance. From a semiclassical

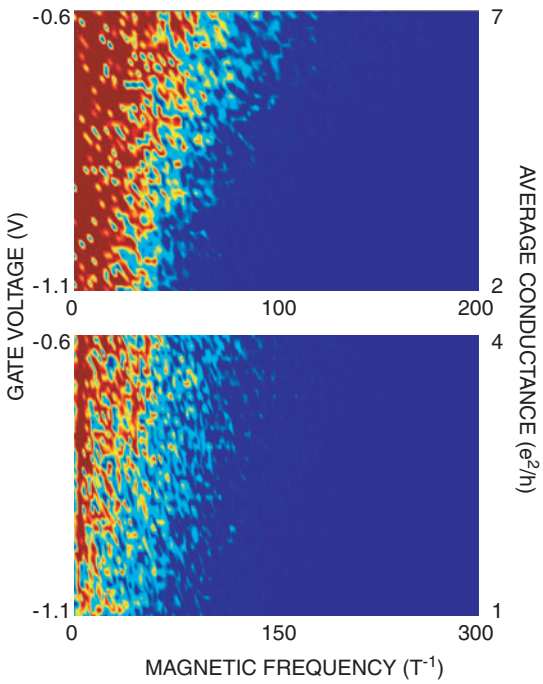

Figure 25. Upper panel: Fourier contour plot constructed from the results of fifty magneto–resistance measurements of the array with dot dimensions of $0.4 \times 0.7\,\mu m^2$. The gate voltage was incremented by 10 mV between successive measurements. Bottom panel: Fourier contour plot constructed from the results of fifty magneto–resistance measurements of the array with dot dimensions of $0.6 \times 1.0\,\mu m^2$. The gate voltage was incremented by 10 mV between successive measurements. A variation from red (dark) to blue (light) corresponds to a change in Fourier amplitude from 5 to 70, respectively.

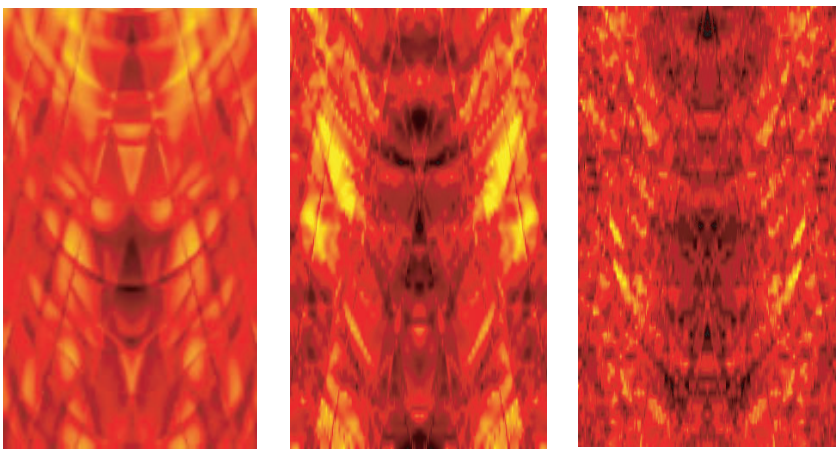

Figure 26. Computed conductance contours for open arrays of one (left), four (middle) and ten (right) quantum dots, respectively. Darker regions correspond to lower conductance, while magnetic field and Fermi energy are plotted on the horizontal and vertical axes, respectively. The magnetic field range is −0.1 to 0.1 T, while the Fermi energy range is 12 to 15 meV.

perspective, this behaviour may be attributed to the fact that the generic phase space for motion in these dots is mixed, rather than fully chaotic [55]. As we have been able to demonstrate, the eigenstates that remain resolved when the dot is open are associated with isolated periodic orbits, which can only be accessed by (classically forbidden) dynamical tunnelling. Transport through these orbits essentially involves a resonant-tunnelling process, which is exactly why such a large modulation of the conductance is found to arise from the contribution of individual orbits. Recall that in a double-barrier system, resonant tunnelling is most pronounced when the transmission probability of this individual barriers is small. This allows the tunnelling particle to be efficiently trapped within the well, and to build up interference between its multiply scattered partial waves. In the problem of interest here, the probability to tunnel onto (or off) orbits within the KAM island should be small, since these orbits are classically inaccessible. At resonant energies that satisfy equation (4), an electron that tunnels onto the orbit will therefore undergo many traversals, before eventually escaping after a time, much longer than that required to transit directly across the ends of the dot. That is, the dynamical tunnelling effectively enhances the trapping time within the dot, allowing the energy levels associated with the tunnelling orbits to remain resolved. (A similar picture has recently been discussed by Takagaki and Ploog [72], although these authors did not account for the influence of tunnelling into classically inaccessible orbits.)

The connection between the density of states and the conductance of open dots has also been appreciated by other authors. Persson *et al* [73] investigated the transport properties of circular dots, in both the open- and tunnelling-regimes, and related their observations to the results of calculations of the eigenstates of the circular billiard. As such, they failed to appreciate the non-uniform nature of the level broadening, introduced by the coupling in the open regime. In later theoretical work, however, Zozoulenko and Berggren [74, 75] decomposed the wavefunction of an open square billiard and found this to be dominated by the contribution from a small number of closed-dot states, consistent with the behaviour discussed here. It is worth pointing out here that the closed-dot basis set of eigenstates used by these authors was that of a perfect square, and so did not account for the perturbing influence of the leads on the dot geometry, and it is for this reason that their wavefunction decomposition always contained contributions from at least a number of states. As we saw in our discussion of figures 8 and 9, it is only when the influence of the leads is properly accounted for that the single-eigenstate nature of transport in the open dots is fully appreciated. In later experimental work, Zozoulenko *et al* [76] studied the magneto-transport in an open dot, and showed that this could be analysed in terms of conductance contours, similar to our discussion of figures 11–15.

One of the key findings of our work is that the transport through open quantum dots appears to be dominated by the contribution from a small number of semiclassical orbits, which are thought to be accessed by dynamical tunnelling [32, 47–50, 54]. Transport results due to isolated orbits have also been reported by other authors. Some of the earliest observations of periodic magneto-conductance oscillations were reported in [77, 78], although neither of these studies considered the origin of the observed behaviour in any detail. Christensson *et al* [79] observed evidence for periodic magneto-conductance oscillations, arising from a magnetically focused orbit, in their investigations of the transport in open triangular dots. In another study of a triangular billiard, periodic conductance fluctuations were observed and were argued to be associated with the contribution of a classically inaccessible orbit [80]. These results support our assertion that the semiclassical description of transport in these systems is considerably more complicated than conventional approaches would suggest.

While our discussion thus far has focused exclusively on the nature of transport in open quantum dots, there is nonetheless a strong connection of our results to the issue of transport in tunnel-coupled dots. As was mentioned in the introduction, current flow through

these structures is dominated by the effect of single-electron tunnelling. In semiconductor quantum dots, the separation between successive dot levels may be comparable to the Coulomb charging energy, and a strong variation of the tunnelling current is observed as the occupation number of the dot is varied [3, 6, 7]. Stopa [81], and more recently Silvestrov and Imry [82], have related this behaviour to strongly scarred wavefunction states of the dots that modulate the tunnel conductance, due to the very different overlap they exhibit with the lead regions.

3.6.2. Generic wave properties of open quantum dots. While our discussion thus far has focused on the semiclassical interpretation of transport in the open dots, there are many aspects of this behaviour that may equivalently be viewed as manifestations of quite generic wave phenomena. A clear demonstration of the wave-mechanical character of transport in the dots is provided by analogue studies of the transmission properties of microwave cavities [15, 83]. The basis for such studies is provided by the exact correspondence between the Schrödinger equation for a freely moving electron in a two-dimensional billiard, and the Helmholtz equations for a microwave resonator [14, 84]. According to this correspondence, the electric field within the classical resonator may be viewed as analogous to the wavefunction of the quantum-mechanical system, while the Landauer–Büttiker formalism provides a direct connection between the transmission properties of the resonator and the conductance of the dot. In a recent study by Kim *et al* [15], the behaviour of an open cavity resonator was compared directly to the results of measurements of an open quantum dot. The results of their study are shown in figure 27, where the frequency dependence of the transmission coefficient of the microwave cavity and the magneto–resistance of the quantum dot are plotted. For the purpose of comparison, the abscissa axes of the two plots have been converted onto the so-called Weyl axis, on which energy is normalized to the average level spacing (Δ) [15]. With this normalization, it is clear that the two plots of figure 27 exhibit strikingly similar behaviour, providing a clear demonstration of the fact that transmission through open quantum dots may be viewed as a wave-mechanical process. Rastering an antenna over the area of the cavity, and measuring the resulting variation of the electrostatic potential, it is actually possible to map out the wavefunction of the cavity [14, 85]. The results of the study of Kim *et al* are shown in figure 28, where we see clear evidence for wavefunction scarring, reminiscent of the behaviour found in the open dots (figures 17–20). Similar to behaviour exhibited by the dots, the scars were found to recur as the frequency was varied, in correspondence with the presence of specific frequency components in the associated transmission fluctuations [15]. Electromagnetic cavity resonators are also realized in vertical-cavity surface-emitting lasers (VCSELs), and Chen *et al* [17] have used such structures to explore field distributions near the lasing threshold. They find the presence of optical modes with strongly scarred field distributions, which they associate with the interference of a small number of eigenstates of a perfectly square cavity. The presumption here is that inevitable imperfections in the VCSEL geometry cause its eigenstates to correspond to a mixture of a small number of states of the pure square, just as we have discussed in the context of figures 7–9. In their report, Chen *et al* provide support for this argument by constructing wavefunctions that are scarred by single orbits, using superpositions of small numbers of basis states of the square.

In figure 10, we saw that, while increasing the width of the dot leads gave rise to strong broadening of many of the dot eigenstates, a small group of states remained almost unaffected by this process. Such behaviour is also observed in studies of microwave cavities, where it is referred to as the phenomenon of resonance trapping (for a review see [86], [87]) (figure 29). Similar to the behaviour that we have discussed, it is found that opening the cavity gives rise to a non-uniform broadening of its eigenstates. In particular, as the width of the cavity opening

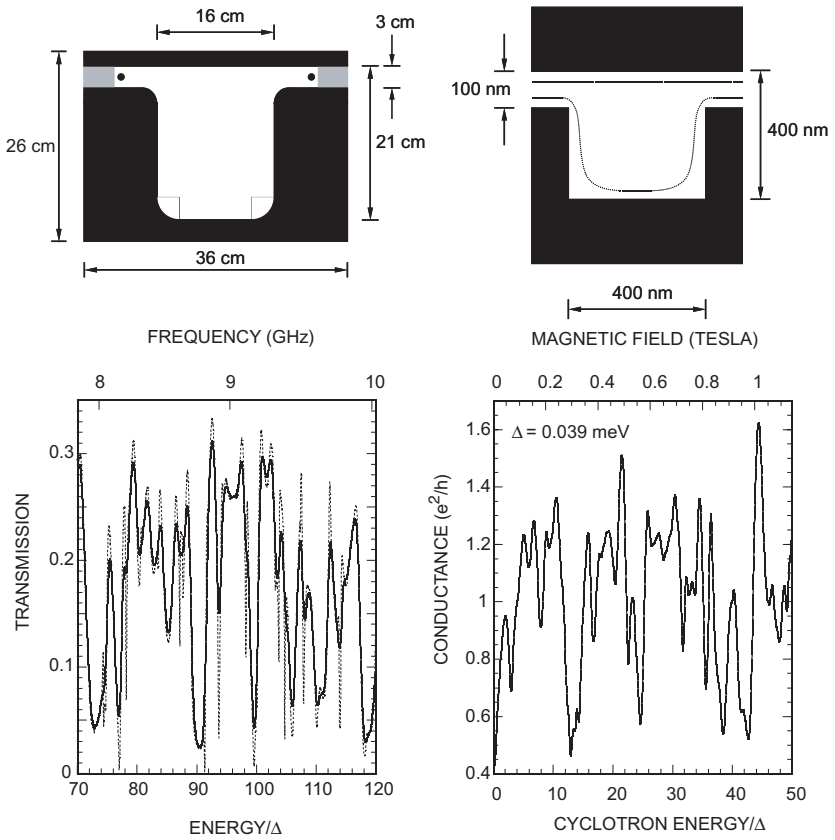

Figure 27. Shown top-left are the dimensions of the microwave cavity resonator that is used to model the quantum dot, whose lithographic dimensions are shown in the top-right figure. The dotted lines indicate schematically the shape of the actual quantum dot that is formed in the 2DEG. The bottom-left figure shows the variation of microwave transmission with frequency, while the bottom-right figure shows the measured magneto–resistance of the quantum dot. Figure reproduced with permission from [15]. Copyright, American Physical Society (2002).

is increased, the lifetime broadening of certain eigenstates actually found to decrease. This is the effect of resonance trapping, and evidence for this can even be seen in the lower panel of figure 10, in which the state at $E/\Delta \approx 139$ appears to become more clearly resolved as the width of the leads is increased.

While the quantum dots that we study are open systems, the scarred states that arise in these structures may be viewed as analogous to standing-wave modes. The manner in which such modes may be excited by an incoming wave is illustrated in figure 29, which essentially shows a set of snapshots of the wavefunction, taken at a series of different times subsequent to injection into the dot [41]. In the case considered here, the Fermi velocity of the electrons is such that the transit time across the dot is only of order a few picoseconds. As can be seen from figure 29, however, the scar is only built up when the electron remains trapped within the dot for sufficient time to be multiply scattered from its potential boundaries. This figure also provides a clue as to the origin of the dynamical tunnelling that we have discussed. While the final scar appears to be decoupled from either of the leads, it is clear from this figure that the initial diffraction of the electron, as it is injected into the dot, sets up the interference conditions

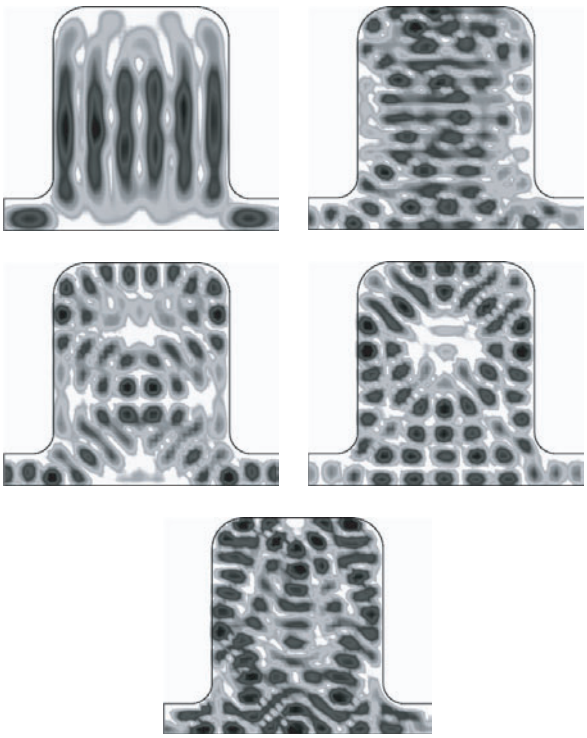

Figure 28. Examples of scars in the microwave cavity resonator. Figure adapted with permission from [15]. Copyright, American Physical Society (2002).

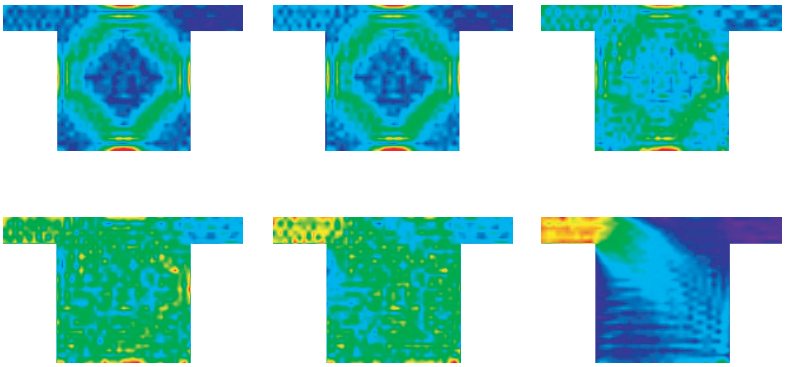

Figure 29. Calculated probability density in a 0.3 μm quantum dot at a magnetic field of 0.28 T. Lighter regions correspond to enhanced probability density and calculations are performed for different values of the phase-breaking time. From top-left to bottom-right, $\tau_\phi = \infty$, 500 ps, 100 ps, 50 ps, 10 ps, and 1 ps, respectively. Viewed in reverse sequence, this figure may be considered as illustrating the time-dependent growth of the wavefunction scar within the quantum dot. Figure reproduced from [41].

that give rise to the formation of the scar. Such behaviour is well known from the study of the wave modes that arise in fluid systems containing arrays of cylinders [16], and is important in the design of mechanical structures such as oil rigs, where one seeks to minimize the influence of resonances due to such standing modes.

Another interesting connection of this work has been noted by Kun *et al* [88] in their studies of hyperdeformed nuclear systems. In investigations of this type, the decay of nuclei from some excited state is studied, as a function of the initial excitation energy. While it is typical to expect a Wigner-like distribution of intermediate states, experiment actually reveals the existence of highly stable modes of motion in the intermediate system, which are excited at quite specific energies. Clearly, there is a strong analogy here to the behaviour exhibited by the open dots that we study, which exhibit long-lived quasi-bound states at certain values of the Fermi energy.

4. Decoherence and interactions in open quantum dots

In section 3, we explored the details of transport in open dots at low temperatures, where the discreteness of the level spectrum can be experimentally resolved. With increasing temperature, however, we expect that electron phase-coherence will be suppressed, and that thermal smearing of the energy levels will ultimately render them unobservable. Indeed, we have already seen that the conductance fluctuations, associated with the discrete density of states, are typically washed out as the temperature is increased above a few degrees kelvin (figure 5). In this section of our review, we consider the factors that contribute to this thermal averaging, and discuss how the temperature-dependent details of transport may be used to infer important information on the behaviour of a key transport parameter, namely the electron phase-breaking time.

4.1. Dephasing in open dots

One of the key parameters for the discussion of transport in mesoscopic systems is the electron phase-breaking time (τ_ϕ), which may be thought of as the average time over which the electron is able to propagate as a coherent wave, before its phase evolution is disrupted though its interaction with its environment [27]. Among the possible sources of dephasing in condensed-matter systems include electron–electron, electron–phonon, and electron–photon, scattering, each of which mechanisms is expected to have a quite distinct dependence on energy. At the low temperatures of interest here, it is usually assumed that the electron–electron interaction is the dominant source of decoherence, although the role of the electron–photon interaction has recently attracted increasing attention [89]. Studies of the temperature dependence of the phase-breaking time provide a valuable means to investigate the relative importance of these mechanisms, and to investigate how phase-coherence is modified by confining electrons in mesoscopic structures, such as quantum dots.

Among the experimental methods that have been employed to determine the value of τ_ϕ in quantum dots, Marcus and co-workers [70, 71, 90, 91] have developed a number of approaches that are based on an assumption of fully chaotic electron scattering in the dots. As we have seen, however, the typical classical phase space in these dots is mixed, rather than fully chaotic, which is known to give rise to very different escape dynamics than that characteristic of chaotic scattering [55]. For this reason, we have used a different approach to determine the value of the phase-breaking time, which is based on the evolution of the magneto-conductance in the high-field, edge-state, regime [92–95]. The key observation in this regime is that the basic field scale of the conductance fluctuations increases once the magnetic field is raised such that the cyclotron-orbit size fits within the dot (figure 30). At such magnetic fields, the fluctuations in the conductance may be thought of as arising from the interference of different skipping-orbits, associated with the populated Landau levels of the sample. To compute the characteristic magnetic flux enclosed by these skipping orbits, consider the area that a single orbit encloses

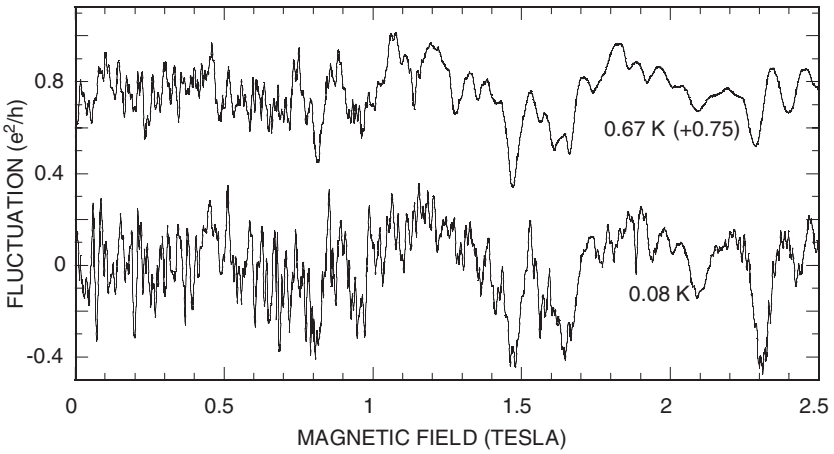

Figure 30. Conductance fluctuations in a 1 μm quantum dot at two distinct temperatures (the higher temperature trace has been shifted upwards by $0.75e^2/h$ for clarity). Figure reproduced with permission from [92]. Copyright, American Physical Society (1995).

as it skips coherently along the walls of the dot [96]:

$$A_\varphi = n_\mathrm{b}\frac{\pi r_\mathrm{c}^2}{2} = v_\mathrm{F}\tau_\varphi r_\mathrm{c}, \tag{7}$$

where n_b is the number of bounces the electron makes before losing phase-coherence, $r_\mathrm{c} = \hbar k_\mathrm{F}/eB$ is the cyclotron radius, and v_F is the Fermi velocity. From this definition, it is possible to obtain a simple expression, relating the average period of the magneto-conductance fluctuations to the magnetic field:

$$B_\mathrm{c}(B) = \frac{\phi_o}{A_\varphi} = \frac{h}{eA_\varphi} = \frac{8\pi^2 m^*}{hk_\mathrm{F}^2\tau_\varphi}B. \tag{8}$$

The field scale here (B_c) is more rigorously defined as the correlation field of the conductance fluctuations, and may be obtained directly from their correlation function:

$$F(\Delta B) = \langle \delta g(B)\delta g(B+\Delta B)\rangle, \qquad F(B_\mathrm{c}) \equiv \tfrac{1}{2}F(0). \tag{9}$$

According to equation (8), when the phase-breaking time is independent of magnetic field, B_c is expected to increase linearly with the magnetic field. Such behaviour is indeed found in experiment (figure 30), and, from the slope of the resulting straight line fit (figure 31, inset), it is possible to use equation (8) obtain an estimate for the phase-breaking time.

In figure 31, we show the measured temperature dependence of the phase-breaking time, obtained in studies of two different quantum dots using the approach of equation (8). There are several features of this figure that are worthy of comment. The first is that, at temperatures around a degree kelvin, the phase-breaking time increases with decreasing temperature, with a power-law form close to $\tau_\phi \propto T^{-1}$. As other authors have noted [71, 90], this variation is reminiscent of that predicted [97] for dephasing by electron–electron scattering with small-energy transfer in two-dimensional disordered systems. Whether this mechanism is responsible for the variation of τ_ϕ observed in the dots remains to be determined, however, although Huibers *et al* [90] have noted that the magnitude of τ_ϕ in these structures is inconsistent with the predictions of this theory. As the temperature is lowered below a degree kelvin, it can be seen in figure 31 that the variation of τ_ϕ deviates from a simple power-law form, and ultimately saturates at the lowest temperatures. The origin of this saturation remains the source

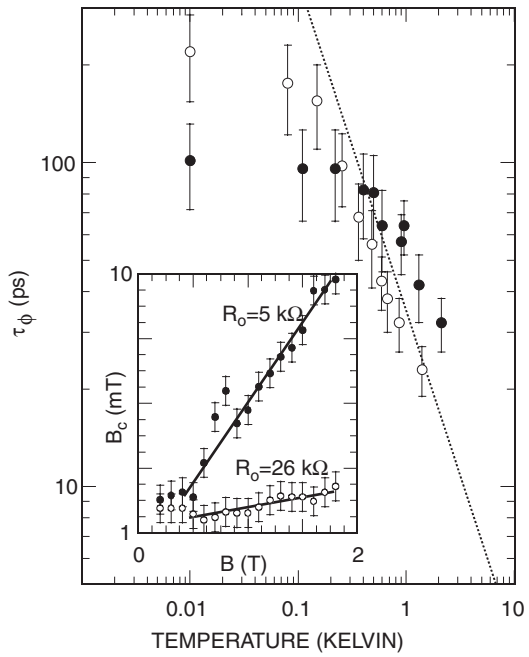

Figure 31. Main panel: measured variation of the phase-breaking time with temperature in a 1 μm (○) and a 0.6 μm (●) split-gate quantum dot. The inset shows the variation of B_c with magnetic field in a 0.4 μm dot at two different gate voltages.

of considerable debate in the literature, although in a recent study we were able to show that the details of the saturation are sensitive to the total electron number in the dot [94]. The other feature of figure 31 that is worth emphasizing is that the value of the phase-breaking time in the saturated regime is several orders of magnitude larger than the typical time required to ballistically traverse the length of the dot. As can be seen from figure 29, such long-term coherence is crucial to the observation of effects associated with the wavefunction scarring.

4.2. Temperature-dependent transport and the signatures of interactions in open dots

The picture of transport that we have presented thus far is essentially based on a single-particle description, which neglects the effects of complicated many-body interactions. While this certainly appears to provide a good description of transport in the open dots, we nonetheless note that the dynamical-tunnelling behaviour that we have discussed implies the existence of certain resonant energies, at which electrons remain quasi-bound in the dot for very long times. For this reason, it might be expected that corrections to the single-particle transport should arise, due to charging of the dot associated with the formation of these resonant states. In this section, we explore this possibility by discussing the results of studies of the temperature-dependent transport characteristics of the open dots, and present evidence for an enhanced electron–electron interaction at low temperatures that is induced by the confining potential of the dots.

4.2.1. Experimental observations. To explore possible signatures of electron interactions in transport, we have investigated the temperature dependence of the conductance in open-dot

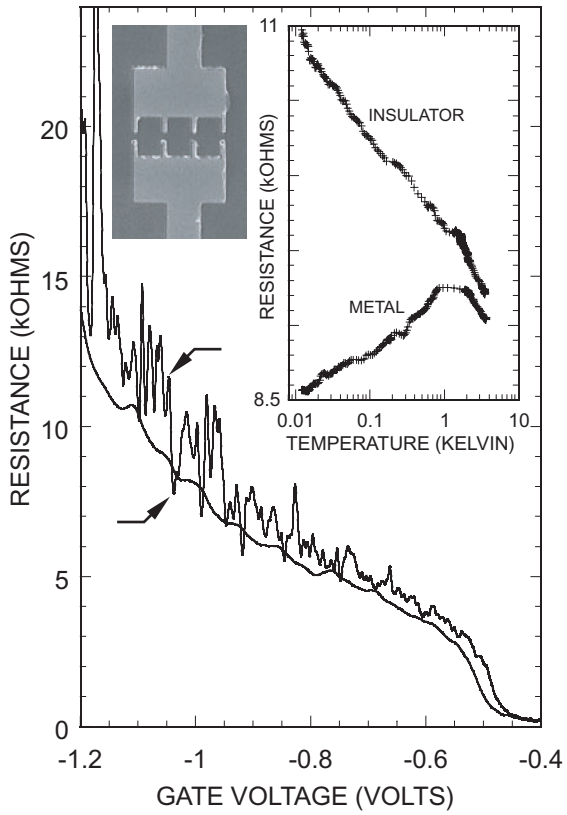

Figure 32. Main panel: gate-voltage characteristic of a three-dot quantum-dot array. The smooth curve was obtained at 3 K, while the fluctuating one was measured at 0.01 K. The left inset shows an SEM micrograph of a similar array. The right inset shows the variation of resistance with temperature, measured at the two gate voltages indicated by arrows in the main panel. Figure reproduced with permission from [38]. Copyright, American Physical Society (2001).

systems [38–40, 98, 99]. The key observation in these studies is illustrated in figure 32, in the main panel of which we show the gate-voltage dependent variation of the resistance, measured in a split-gate quantum-dot array at two different temperatures. As we have discussed already, the oscillations in the low temperature curve result as the gate-voltage variation sweeps the discrete energy states of the open structure past the Fermi level. In the inset to figure 32, we show the temperature-dependent variation of the resistance, obtained by setting the gate voltage to correspond to a local maximum or minimum in the low-temperature data (as indicated by the arrows in the main panel). The data sets in this inset show two distinct regimes of temperature-dependent behaviour, which have been found to be quite generic to all local maxima and minima in the low-temperature conductance. First, we note that both data sets show an initial increase in resistance, as the temperature is lowered to around a degree kelvin. At lower temperatures than this, however, a crossover to a logarithmic variation occurs, the sign of which is opposite for the local resistance minimum and maximum. In this sense, the data of figure 32 appear to show evidence for a metal–insulator transition, which occurs at temperatures where the discrete level spectrum of the dot should be resolved.

Based on studies of the temperature-dependent behaviour in several different devices, we have suggested that the initial increase of the dot resistance with decreasing temperature is

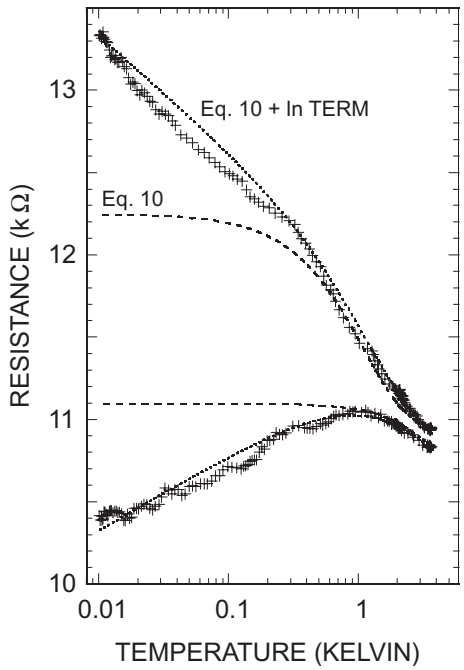

Figure 33. Measured variation of resistance with temperature in a split-gate quantum-dot array. The dashed lines are fits to the form of equation (10) while the dotted line area fits to equation (10) with an additional log term added. Figure adapted with permission from [40]. Copyright, American Institute of Physics (2002).

fitted by the following form [99]:

$$G \propto \Delta G \exp\left[-\left(\frac{T_0}{T}\right)^p\right]. \tag{10}$$

In figure 33, fits to the form of equation (10) have been performed for a set of metallic and insulating points (see the dashed lines). At least in the temperature range of a few degrees kelvin, the observed variation of the resistance is well described by equation (10). Exponential variations of the form of equation (10) are well known from studies of the metal–insulator transition in two-dimensional systems (for a recent review, see [100]), in which they are usually associated with a transport process that involves the excitation of carriers across some characteristic energy gap ($k_B T_0$). One feature of the exponential dependence that should be noted here, is that it occurs over the same range of temperature for which the conductance fluctuations become observable in the magneto–resistance (see, e.g. figure 5). Since the fluctuations themselves represent a signature of the discrete density of states of the dots, we have previously suggested that the exponential resistance variation of equation (10) is associated with a transition from thermally broadened, to energetically resolved, dot levels [39]. The suggestion is that, as the temperature is lowered and these levels become resolved, transport requires the excitation of carriers across an associated energy gap. At least consistent with this, typical values for the activation temperature T_0 are found to be of order a few degrees kelvin, which seems quite reasonable given the typical level splitting expected in these dots [99].

As the temperature is lowered below a degree kelvin, an additional contribution to the resistance emerges, which, as we show in figures 32 and 33, varies logarithmically with

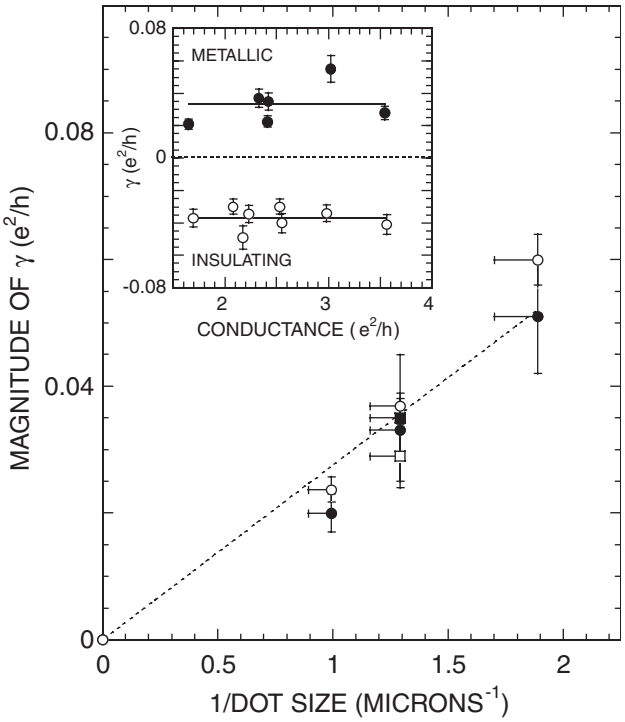

Figure 34. Main panel: magnitude of the parameter γ and its scaling as a function of inverse dot size. Filled symbols correspond to metallic points while open symbols correspond to insulating points. The square symbols represent data points obtained in the presence of a static perpendicular magnetic field of 0.1 T. Inset: variation of γ for a number of different metallic (●) and insulating (○) states, obtained in measurements of a three-dot quantum-dot array. Figures reproduced with permission from [38]. Copyright, American Physical Society (2002).

temperature. For a quantitative analysis of this dependence, we write the variation of the conductance at low-temperatures as $G \propto \gamma \ln(T)$. From studies of the temperature dependence of the resistance of numerous metallic and insulating states, we have found the magnitude of γ to be essentially the same in both the metallic and the insulating regimes (see the inset of figure 34), and to be relatively insensitive to the average conductance (i.e. the gate voltage). We have found evidence for a well-defined scaling of γ with dot size, however, which we illustrate in figure 34. In this figure, we plot the average values of γ, obtained from measurements made at more than fifty different gate voltages in three different structures, as a function of inverse dot size. The additional point, at the origin of this figure, was obtained from measurements performed on a structure with its gates held grounded, in which case the relevant electron system is the heterojunction 2DEG. This situation essentially corresponds to the limit of infinite dot size, and in this case we find no evidence for a logarithmic variation [38, 99]. For the range of dot sizes considered here, the scaling in figure 34 appears to correspond to an inverse dependence on dot size.

A clue as to the origin of the logarithmic term is provided by its insensitivity to the application of moderate magnetic fields. This property is apparent in figure 34, where we use the open and filled square symbols to represent the average values of γ, determined from temperature-dependent studies in the presence of a static magnetic field of 0.1 T. The magnetic field was applied perpendicular to the plane of the 2DEG, and should be sufficiently

large to break electron time-reversal symmetry. In spite of this, however, the data points plotted in figure 34 show that, at least within our experimental accuracy, the value of γ is not affected by the breaking of this symmetry. Such invariance is reminiscent of the behaviour found in studies of disordered films and wires, in which the conductance corrections due to electron interactions are known to be insensitive to the presence of symmetry-breaking magnetic fields (for an extensive review, see [101]). In fact, we have suggested that the size-dependent scaling of the logarithmic term in figure 34 is consistent with an effect in which the boundary interactions of the electrons act to amplify their mutual repulsion. While in an unconfined system the mutual repulsion between any two electrons will tend to drive them apart from each other, in a mesoscopic structure the carriers are reflected at the confining boundaries and are forced to interact more strongly with each other. This boundary interaction should become more important as the system size is reduced, and we expect that its relative influence should scale in inverse proportion to the perimeter of the structure, which is actually consistent with the scaling behaviour found in figure 34.

4.2.2. Theoretical modelling. The suggestion of the experimental studies in section 4.2.1 is that the additional, logarithmic, term in the resistance arises from confinement-enhanced of the electron–electron interaction [38]. For this reason, we have formulated [40, 102] a many-body description of transport in open dots that is based on the idea of the Anderson system, in which a single impurity level with an on-site electron–electron interaction is coupled to a one-dimensional lead [103–107]. In our case, the single impurity is interpreted as the quantum dot, which is coupled to two quantum-point-contact leads. While the detailed formation of this model is described in [102], we obtain a many-body model for the interacting open system by starting from the single-particle eigenbasis of the integral dot/lead system, assuming just one lateral mode. The propagating one-dimensional eigenstates of this system are identified by their wavenumber (k) in the point-contacts. At certain energies, we have seen (figure 8) that the transmission of this mode can exhibit a Fano-type resonance, reflecting the formation of a quasi-bound state, as we have discussed. In this situation, we assume that the resulting effective-interaction matrix elements will also exhibit a resonance and the model Hamiltonian which should describe this interaction for one mode propagating through a single open dot may be written as [102]:

$$\hat{H} = -\beta \left[\sum_{k,\sigma} (\varepsilon_{k\sigma} - \mu_k) c^+_{k\sigma} c_{k\sigma} + \frac{1}{2} \sum_{(k\sigma)\neq(k'\sigma')} V_{(k\sigma)(k'\sigma')} c^+_{k\sigma} c_{k\sigma} c^+_{k'\sigma'} c_{k'\sigma'} \right], \tag{11}$$

where $\beta = 1/k_{\mathrm{B}}T$, μ_k is the electrochemical potential associated with the mode with wavenumber k, σ denotes the usual spin index, $c^+_{k\sigma}/c_{k\sigma}$ are the usual creation/annihilation operators, and $\varepsilon_{k\sigma}$ denotes the single-particle dispersion relation. The applied voltage between the injecting electron reservoirs corresponds to the difference in chemical potentials, $\mu_{k>0} - \mu_{k<0}$. For the effective-interaction matrix that enters the Hamiltonian, we employ the following peaked expression in the vicinity of a resonance (E_0):

$$V_{(k\sigma)(k'\sigma')} \propto (U - \delta_{\sigma\sigma'} U^{\mathrm{ex}}) \frac{\Gamma^2}{(\varepsilon_k - E_0)^2 + \Gamma^2} \frac{\Gamma^2}{(\varepsilon'_k - E_0)^2 + \Gamma^2}. \tag{12}$$

Here, U and U^{ex} are the Hartree and exchange terms, respectively, and 2Γ denotes the total width of the interaction resonance, corresponding to the lifetime of the resonantly trapped charge. Note here that screening within any particular mode is included explicitly in this many-body Hamiltonian, whereas screening effects arising from propagating background

modes, and the environment, are assumed to be contained within the effective-interaction matrix V.

To calculate transport properties from this model, we consider the diagonal non-equilibrium (due the non-constant chemical potential) many-body density-matrix. For numerical reasons, the continuum of k-states is discretized in our simulations, and we further employ a mean-field approach for the calculation of occupation numbers for state-numbers larger than 16 (The discretization in k-space must be chosen such that the resulting energy-spacing is small compared to $k_{\mathrm{B}}T$ [102]). The current flowing through the system (and hence the conductance) can then be expressed in terms of the single-particle transmission probability (with its Fano-type resonance) and the occupation numbers [102]. In the inset to figure 35, we show the typical dependence of the conductance correction due to the interaction (assuming unity transmission) with varying chemical potential and temperature. The conductance valley, apparent in this figure, can be understood as arising from a depletion of current-carrying k-states at energies below that at which the peaked interaction occurs. After the interaction has been overcome by the chemical potential, an enhanced density of states contributes to the current, and a conductance peak now results. A systematic analysis [102] leads us to define the characteristic energy scale $k_{\mathrm{B}}T^{*}_{G,R} = \alpha^{G,R}(\Gamma V^{\mathrm{state}}_{\mathrm{tot}})^{0.5}$, with fitting parameters $\alpha^{G} \approx 0.55$ and $\alpha^{R} \approx 0.31$ for the conductance and resistance maxima, respectively. $V^{\mathrm{state}}_{\mathrm{tot}}$ denotes the normalized interaction energy per state, and we note that the temperature $T^{*}_{G,R}$ has a form reminiscent of an effective Kondo temperature.

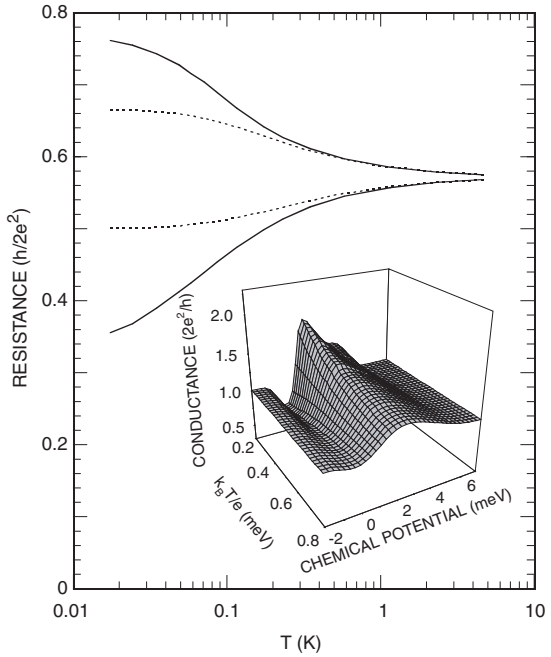

Figure 35. Computed temperature dependence of the resistance peak (upper curve) and valley associated with a specific peaked interaction. The calculation includes 128 k-states and the solid lines correspond to the case where interactions are included, while the dotted lines are for no interaction. The inset shows the normalized conductance as a function of the chemical potential μ_k (relative to E_0) and the temperature T for $\Gamma = 0.4$, $U = 2.4$, $U^{\mathrm{ex}} = 0.6$ (with a total number of 12 k-states). Figure adapted with permission from [40]. Copyright, American Institute of Physics (2002).

At high-temperatures (i.e. when $T \gg T^*_{G,R}$), we find a modified Boltzmann law for the scaling of the corrections to the local conductance and resistance peaks:

$$G^{\rm corr}_{\rm peak} \propto \exp\left[\left(\frac{T^*_G}{T}\right)^2\right], \qquad R^{\rm corr}_{\rm peak} \propto \exp\left[\left(\frac{T^*_R}{T}\right)^2\right]. \tag{13}$$

In the limited temperature range near $T \approx T^*_{G,R}$, however, a conductance variation close to $\ln T$ is found, similar to the behaviour found in experiment.

To compare the predictions of this peaked-interaction model with experiment, we show the results of a more realistic simulation in the main panel of figure 35, which now includes the Fano-type resonance (figure 8) in the single-particle transmission probability. Here, we have taken $\Gamma = 0.02\,\text{meV}$, $U = 0.125\,\text{meV}$, and $U^{\rm ex} = 0.5U$, a parameter choice which yields $V^{\rm state}_{\rm tot} \approx 0.010\,\text{meV}$, $T^*_G \approx 95\,\text{mK}$ and $T^*_R \approx 53\,\text{mK}$. We have also assumed a Fano-like transmission probability with a peak at $E_{\rm p} = \Gamma$, a zero at $E_0 = 0$, a total amplitude prefactor of 0.5, and a background transmission of 0.5. Furthermore, we have assumed that we have one non-resonant background mode (with a conductance of $2e^2/h$). The dotted curves in figure 34 show the variation of the peak- and valley-resistance values as a function of the temperature, which were computed without the inclusion of any interaction terms (i.e. this figure shows the temperature behaviour due to the single-particle Fano-resonance of the mode). The solid lines in the figure correspond to the situation where the peaked interaction term has been included in the simulation. Clearly, the interaction yields an increased fluctuation amplitude, compared to the single-particle behaviour. In the limited temperature range close to $T^*_{G,R}$, one can see a log-like correction due to the peaked interaction, as a first-order correction beyond the single-particle case. The qualitative similarity with the experimental results of figure 33 is suggestive, and a further interesting observation is that the interaction corrections to the resistance valley (i.e. conduction peak) onset at higher temperatures than for the resistance peak, which can also be seen in the experiment. The agreement between experiment and theory is by no means complete, however. While, for ease of implementation [102], we have investigated the behaviour for a single propagating mode, in experiment one typically deals with structures in which many propagating modes, and temperature-dependent dephasing effects, are present. To conclusively associate the features observed in experiment with many-body effects, it will therefore be necessary to extend this model to account for these differences. This having been said, however, we are encouraged by the fact that our rather simple model does indeed yield interaction-induced corrections to the conductance of open dots.

5. Conclusions

In this review, we have seen that the study of electron transport in open quantum dots yields a rich variety of behaviour, an understanding of which requires a proper treatment of the wave-mechanical properties of the electron. At the same time, we have also seen that these structures provide an ideal system for investigating the semiclassical description of quantum systems. The starting point for the understanding of the transport properties of these devices is the non-uniform broadening of their energy levels, which is generated when the dot is opened to its reservoirs by means of one-dimensional leads. Due to their weak overlap with the leads, a small subset of the closed-dot states develop only a weak broadening when the dot is opened, while the majority of states are broadened beyond recognition. By applying an external magnetic field, or by varying gate voltage and changing the size of the dot, the discrete states can be swept past the Fermi level, giving rise to an associated modulation of the conductance that is observed in experiment at sufficiently low temperatures. A characteristic feature of those eigenfunctions that persist when the dot is opened, is that they tend to be scarred by semiclassical orbits that

buildup probability in the wavefunction at regions located away from the leads. The scarring orbits are typically inaccessible to classical particles injected into the quantum dot, and we have provided evidence that these orbits are accessed by the quantum-mechanical process known as dynamical tunnelling. An important property of the scars is that they are found to recur regularly as the gate voltage or magnetic field is varied, and this property is understood to follow from quantization of the associated semiclassical orbits. At the same time, we have seen that the scars may equivalently be viewed as analogous to standing-wave modes of the electron cavity, which are excited at specific magnetic fields, or gate voltages, when electron waves are injected into the dot. Support for this notion is provided by the striking similarities revealed in analogue studies of the microwave-transmission properties of macroscopic cavity resonators.

The description of transport we have developed here is quite distinct from that which has gained wide acceptance in the literature, where it is typical to assume that the classical dynamics of electrons in the dots is fully chaotic (hyperbolic). While the advantage of such an assumption is that it reduces the semiclassical analysis of transport to an elegant analytical form, it should be emphasized that such convenience is achieved at the cost of a realistic physical description. In particular, we have seen here, and other authors have shown [55–58], that the classical dynamics of these dots is typically mixed, rather than fully chaotic. A characteristic feature of the mixed phase space is the presence of well-defined KAM islands, which correspond to periodic orbits separated from the chaotic sea by classically inaccessible regions of phase space. In this review, we have provided strong evidence that the transport properties of these dots can be dominated by the dynamical tunnelling of electrons onto the KAM islands. It is important to emphasize that no such behaviour is expected in fully chaotic systems, in which all points in phase space are classically accessible. In spite of some widely referenced works, in which differences in the electrical properties were argued to arise for regular and chaotic cavities [77, 78], it is our standpoint that, at least under typical experimental conditions, it is impossible to realize fully chaotic dots. One widely studied indicator of the dynamics is the zero-field peak in the magneto–resistance, which has been ascribed to a weak-localization effect [108]. The lineshape of this peak is predicted to be different for chaotic and regular cavities, and experimental support of these ideas was argued for in [78]. In numerical studies, however, we have found that the lineshape of this peak can have little to do with the underlying classical dynamics [109, 110], and our basic viewpoint is that the transport properties of these dots are, in fact, dominated by their regular orbits.

While strong support for the role of dynamical tunnelling in transport has been provided here, the detailed mechanism that gives rise to this effect remains to be determined. In recent studies of this effect in cold-atom systems, the tunnelling between different KAM islands was argued to be mediated by the presence of the chaotic regions of phase space in which the islands are embedded [65]. It is not clear, however, if such chaos-assisted tunnelling is relevant here, where the strong diffraction of electrons, that is generated as they are injected into the dot, must be taken into account [48]. The role of such diffraction effects has also been considered by other authors [111], and an important task in future work will be to develop a description of transport that properly accounts for the dynamical tunnelling.

While the split-gate dots on which we have focused are characterized by the presence of soft walls, it should be noted that our conclusions are not restricted to such structures. In fact, similar behaviour to that discussed here has also been found in numerical studies of hard-walled dots [41, 47, 48], and in microwave cavities [15], which may essentially be viewed as hard-walled due to the short skin depth at microwave frequencies. Regular conductance oscillations, with similar characteristics to those which we have discussed, have also been found in experimental investigations of etched dots [112, 113], which are expected

to exhibit much harder walls. These observations demonstrate that the key requirement for the occurrence of dynamical tunnelling is the presence of a dot geometry that gives rise to classically mixed dynamics. In this sense, it is not surprising that our observations should turn out to be so general, since mixed systems tend to be the rule in nature, rather than the exception.

In much of our discussion, we have essentially relied upon a single-particle treatment of transport, which neglects the influence of many-body interactions (although we have included self-consistency in our calculations of realistic device profiles). In spite of this, we have seen that we have been able to account successfully for many details of the transport in the open dots. At the lowest experimental temperatures, however, we have observed a logarithmic correction to the conductance which we have suggested is associated with the influence of electron interactions. The magnitude of this term is insensitive to the application of modest magnetic fields, and its amplitude increases inversely with dot size. In an attempt to account for this behaviour, we have developed a many-body model of transport, based on the premise that the Coulomb interaction can be peaked at certain energies, which correspond to the formation of the scarred wavefunction states. While this model requires further refinement, it does at least provide evidence for corrections to the conductance of open dots, arising from many-body interactions. In this sense, the study of dynamical tunnelling in mesoscopic structures offers the potential of observing new phenomena, associated with the many-body interactions that arise during the tunnelling. We have considered, for example, the possibility that the dynamical tunnelling might give rise to some sort of Kondo effect [114]. Quite generally, an important requirement for observation of the Kondo effect is the presence of a localized spin that is able to interact with a reservoir of conducting electrons. In the particular system of interest here, we have seen that electrons may tunnel into isolated orbits, where they remain trapped for a very long time before ultimately escaping from the dot. These orbits may therefore be viewed as the analogue of the localized charge in the classic Kondo effect, and may interact with other electrons that are more freely transmitted through the dot. Indeed, the logarithmic variation that we observe, of the dot conductance with temperature, is strikingly reminiscent of that found in the Kondo effect. Since Kondo physics has recently been proposed as the origin of the so-called '0.7 structure' in quantum point contacts [115, 116], it only seems reasonable to also consider its possible manifestations in open dots.

Acknowledgments

Much of the work discussed in this review was undertaken in collaboration with a number of colleagues. We would particularly like to acknowledge the valuable contributions made by A Andresen, N Aoki, Y Aoyagi, M Barth, J Cooper, M Elhassan, F Ge, K Ishibashi, Y-H Kim, L-H Lin, Y Ochiai, D P Pivin, Jr, C Prasad, A Shailos, H-J Stöckmann, Y Takagaki, and D Vasileska. We would also like to express our appreciation for the financial support for this research, which has been provided by the Office of Naval Research (JPB and DKF) and the Department of Energy (JPB).

References

[1] Datta S M 1995 *Electronic Transport in Mesoscopic Systems* (Cambridge: Cambridge University Press)
[2] Kelly M J 1995 *Low-Dimensional Semiconductors* (Oxford: Oxford University Press)
[3] Ferry D K and Goodnick S M 1997 *Transport in Nanostructures* (Cambridge: Cambridge University Press)
[4] Davies J H 1998 *The Physics of Low Dimensional Semiconductors* (Cambridge: Cambridge University Press)
[5] Beenakker C W J and van Houten H 1992 *Solid State Phys.* **44** 1

[6] Kouwenhoven L P, Marcus C M, McEuen P L, Tarucha S, Westervelt R M and Wingreen N S 1997 *Mesoscopic Electron Transport* ed L P Kouwenhoven *et al* NATO ASI, Ser. E, (Dordrecht: Kluwer)
[7] Bird J P (ed) 2003 *Electron Transport in Quantum Dots* (New York: Kluwer/Plenum) submitted
[8] Burkard G, Loss D and DiVincenzo D P 1999 *Phys. Rev.* B **59** 2070
[9] Recher P, Sukhorukov E V and Loss D 2000 *Phys. Rev. Lett.* **85** 1962
[10] Orlov A O, Amlani I, Bernstein G H, Lent C S and Snider G L 1977 *Science* **277** 928
[11] Komiyama S, Astafiev O, Antonov V, Hirai H and Kutsuwa T 2000 *Nature* **403** 405
[12] van der Vaart N C, Johnson A T, Kouwenhoven L P, Maas D J, de Jong W, de Ruyter van Steveninck M P, van der Enden A and Harmans C J P M 1993 *Physica* B **189** 99
[13] Pasquier C, Meirav U, Williams F I B, Glatti D C, Jin Y and Etienne B 1993 *Phys. Rev. Lett.* **70** 69
[14] Stöckmann H-J 1999 *Quantum Chaos—An Introduction* (Cambridge: Cambridge University Press)
[15] Kim Y-H, Barth M, Stöckmann H-J and Bird J P 2002 *Phys. Rev.* B **65** 165317
[16] Evans D V and Porter R 1999 *J. Eng. Math.* **35** 149
[17] Chen Y F, Huang K F and Lan Y P 2002 *Phys. Rev.* E **66** 046215
[18] Bird J P 1999 *J. Phys.: Condens. Matter* **11** R413
[19] Thornton T J, Pepper M, Ahmed H, Andrews D and Davies G J 1986 *Phys. Rev. Lett.* **56** 1198
[20] Nixon J A and Davies J H 1990 *Phys. Rev.* B **41** 7929
[21] Stopa M 1996 *Phys. Rev.* B **53** 9595
[22] Vasileska D, Wybourne M N, Goodnick S M and Gunther A D 1998 *Semicond. Sci. Technol.* **13** A37
[23] Büttiker M 1992 *Semiconductors and Semimetals* vol 35, ed M Reed (New York: Academic) pp 191–277
[24] van Wees B J, Kouwenhoven L P, Harmans C J P M, Williamson J G, Timmering C E, Broekaart M E I, Foxon C T and Harris J J 1989 *Phys. Rev. Lett.* **62** 2523
[25] Stopa M, Bird J P, Ishibashi K, Aoyagi Y and Sugano T 1996 *Phys. Rev. Lett.* **76** 2145
[26] Bird J P, Stopa M, Connolly K, Pivin D M Jr, Ferry D K, Akis R, Aoyagi Y and Sugano T 1997 *Phys. Rev.* B **56** 7477
[27] Lin J J and Bird J P 2002 *J. Phys.: Condens. Matter* **14** R501
[28] McEuen L P, Foxman E B, Meirav U, Kastner M A, Meir Y, Wingreen N S and Wind S J 1991 *Phys. Rev. Lett.* **66** 1926
[29] Ashoori R C, Störmer H L, Weiner J S, Pfeiffer L N, Pearton S J, Baldwin K W and West K W 1992 *Phys. Rev. Lett.* **68** 3088
[30] Tarucha S, Austing D G, Honda T, van der Hage R J and Kouwenhoven L P 1996 *Phys. Rev. Lett.* **77** 3613
[31] Akis R, Bird J P and Ferry D K 2002 *Appl. Phys. Lett.* **81** 129
[32] Bird J P, Akis R, Ferry D K, Vasileska D, Cooper J, Aoyagi Y and Sugano T 1999 *Phys. Rev. Lett.* **82** 4691
[33] Usuki T, Saito M, Takatsu M, Kiehl R A and Yokoyama N 1995 *Phys. Rev.* B **52** 8244
[34] Shao Z, Porod W and Lent C S 1994 *Phys. Rev.* B **49** 7453
[35] Göres J, Goldhaber-Gordon D, Heemeyer S, Kastner M A, Shtrikman H, Mahalu D and Meirav U 2000 *Phys. Rev.* B **62** 2188
[36] Bird J P, Akis R and Ferry D K 1999 *Phys. Rev.* B **60** 13676
[37] Akis R, Bird J P, Vasileska D and Ferry D K 2003 *Electron Transport in Quantum Dots* ed J P Bird (New York: Kluwer/Plenum) submitted
[38] Shailos A *et al* 2001 *Phys. Rev.* B **63** 241302
[39] Shailos A 2001 *Phys. Rev.* B **64** 193302
[40] Indlekofer K M, Bird J P, Akis R, Ferry D K and Goodnick S M 2002 *Appl. Phys. Lett.* **81** 3861
[41] Akis R, Bird J P and Ferry D K 1996 *J. Phys.: Condens. Matter* **8** L667
[42] Christensson L, Linke H, Omling P, Lindelof P E, Zozoulenko I V and Berggren K F 1998 *Phys. Rev.* B **57** 12306
[43] Bøggild P, Kristensen A, Bruus H, Reimann S M and Lindelof P E 1998 *Phys. Rev.* B **57** 15408
[44] Taylor R P, Sachrajda A S, Adams J A, Coleridge P T and Zawadzki P 1993 *Phys. Rev.* B **47** 4458
[45] Ye P D and Tarucha S 1999 *Phys. Rev.* B **59** 9794
[46] Heller E J 1984 *Phys. Rev. Lett.* **53** 1515
[47] Akis R, Ferry D K and Bird J P 1997 *Phys. Rev. Lett.* **79** 123
[48] Akis R, Ferry D K and Bird J P 1996 *Phys. Rev.* B **54** 17705
[49] Bird J P, Ferry D K, Akis R, Ishibashi K, Aoyagi Y, Sugano T and Ochiai Y 1996 *Europhys. Lett.* **35** 529
[50] Bird J P, Akis R, Ferry D K, Aoyagi Y and Sugano T 1997 *J. Phys.: Condens. Matter* **9** 5935
[51] Akis R, Bird J P, Ferry D K, Vasileska D, Cooper J, Aoyagi Y and Sugano T 2000 *Physica* E **7** 740
[52] Akis R, Bird J P, Ferry D K and Vasileska D 2000 *Physica* E **7** 745
[53] Jalabert R A, Baranger H U and Stone A D 1990 *Phys. Rev. Lett.* **65** 2442
[54] de Moura A P S, Lai Y-C, Akis R, Bird J P and Ferry D K 2002 *Phys. Rev. Lett.* **88** 236804

[55] Ketzmerick R 1996 *Phys. Rev.* B **54** 10841
[56] Micolich A P, Taylor R P, Newbury R, Bird J P, Wirtz R, Dettmann C P, Aoyagi Y and Sugano T 1998 *J. Phys.: Condens. Matter* **10** 1339
[57] Sachrajda A S, Ketzmerick R, Gould C, Feng Y, Kelly P J, Delage A and Wasilewski Z 1998 *Phys. Rev. Lett.* **80** 1948
[58] Takagaki Y, Elhassan M, Shailos A, Prasad C, Bird J P, Ferry D K, Ploog K H, Lin L-H, Aoki N and Ochiai Y 2000 *Phys. Rev.* B **62** 10255
[59] Davis M J and Heller E J 1981 *J. Chem. Phys.* **75** 246–54
[60] Bohigas O, Tomsovic S and Ullmo D 1993 *Phys. Rep.* **223** 43
[61] Tomsovic S (ed) 1998 *Tunneling in Complex Systems* (Singapore: World Scientific)
[62] Tomsovic S 2001 *Phys. Scr.* T **90** 162
[63] Dembowski C, Gräf H-D, Heine A, Hofferbert R, Rehfeld H and Richter A 2000 *Phys. Rev. Lett.* **84** 867
[64] Hensinger W K 2001 *Nature* **412** 52
[65] Steck D A, Oskay W H and Raizen M G 2001 *Science* **293** 274
[66] Gutzwiller M C 1990 *Chaos in Classical and Quantum Mechanics* (New York: Springer)
[67] Elhassan M *et al* 2001 *Phys. Rev.* B **64** 085325
[68] Akis R and Ferry D K 1999 *Phys. Rev.* B **59** 7529
[69] Aoki N, Oonishi D, Iwase Y, Ochiai Y, Ishibashi K, Aoyagi Y and Bird J P 2002 *Appl. Phys. Lett.* **80** 2970
[70] Marcus C M, Westervelt R M, Hopkins P F and Gossard A C 1993 *Phys. Rev.* B **48** 2460
[71] Clarke R M, Chan I H, Marcus C M, Duruöz C I, Harris J S Jr, Campman K and Gossard A C 1995 *Phys. Rev.* B **52** 2656
[72] Takagaki Y and Ploog K H 2000 *Phys. Rev.* E **62** 4804
[73] Persson M, Pettersson J, von Sydow B, Lindelof P E, Kristensen A and Berggren K F 1995 *Phys. Rev.* B **52** 8921
[74] Zozoulenko I V, Schuster R, Berggren K F and Ensslin K 1997 *Phys. Rev.* B **55** R10209
[75] Zozoulenko I V and Berggren K F 1997 *Phys. Rev.* B **56** 6931
[76] Zozoulenko I V, Sachrajda A S, Gould C, Berggren K-F, Zawadzki P, Feng Y and Wasilewski Z 1999 *Phys. Rev. Lett.* **83** 1838
[77] Marcus C M, Rimberg A J, Westervelt R M, Hopkins P F and Gossard A C 1992 *Phys. Rev. Lett.* **69** 506
[78] Chang A M, Baranger H U, Pfeiffer L N and West K W 1994 *Phys. Rev. Lett.* **73** 2111
[79] Christensson L, Linke H, Omling P, Lindelof P E, Zozoulenko I V and Berggren K F 1998 *Phys. Rev.* B **57** 12306
[80] Bøggild P, Kristensen A, Bruus H, Reimann S M and Lindelof P E 1998 *Phys. Rev.* B **57** 15408
[81] Stopa M 1996 *Phys. Rev.* B **54** 13767
[82] Silvestrov P G and Imry Y 2000 *Phys. Rev. Lett.* **85** 2565
[83] Blomquist T, Schanze H, Zozoulenko I V and Stöckmann H-J 2002 *Phys. Rev.* E **66** 026217
[84] Richter A 1999 Emerging applications of number theory *The IMA Volumes in Mathematics and its Applications* vol 109, ed D A Hejhal (New York: Springer) pp 479–523
[85] Kuhl U and Stöckmann H-J 1998 *Phys. Rev. Lett.* **80** 3232
[86] Rotter I 1991 *Rep. Prog. Phys.* **54** 635
[87] Persson E, Rotter I, Stöckmann H-J and Barth M 2000 *Phys. Rev. Lett.* **85** 2478
[88] Kun Yu S, Vagov A V and Vorov O K 1999 *Phys. Rev.* C **59** R585
[89] Altshuler B L, Gershenson M E and Aleiner I L 1998 *Physica* E **3** 58
[90] Huibers A G, Switkes M, Marcus C M, Campman K and Gossard A C 1998 *Phys. Rev. Lett.* **81** 200
[91] Huibers A G, Folk J A, Patel S R, Marcus C M, Duruöz C I and Harris J S Jr 1999 *Phys. Rev. Lett.* **83** 5090
[92] Bird J P, Ishibashi K, Ferry D K, Ochiai Y, Aoyagi Y and Sugano T 1995 *Phys. Rev.* B **51** R18037
[93] Bird J P, Micolich A P, Linke H, Ferry D K, Akis R, Ochiai Y, Aoyagi Y and Sugano T 1998 *J. Phys.: Condens. Matter* **10** L55
[94] Pivin D P Jr, Andresen A, Bird J P and Ferry D K 1999 *Phys. Rev. Lett.* **82** 4687
[95] Prasad C, Ferry D K, Shailos A, Elhassan M, Bird J P, Lin L-H, Aoki N, Ochiai Y, Ishibashi K and Aoyagi Y 2000 *Phys. Rev.* B **62** 15356
[96] Ferry D K, Edwards G, Yamamoto K, Ochiai Y, Bird J P, Ishibashi K, Aoyagi Y and Sugano T 1995 *Japan. J. Appl. Phys.* **34** 4338
[97] Altshuler B L, Aronov A G and Khmelnitskii D E 1982 *Phys. J.* C **15** 7367
[98] Lin L-H 1999 *Phys. Rev.* B **60** R16299
[99] Andresen A 1999 *Phys. Rev.* B **60** 16050
[100] Abrahams E 1999 *Ann. Phys.* (Leipzig) **8** 539
[101] Lee P A and Ramakrishnan T V 1985 *Rev. Mod. Phys.* **57** 287

[102] Indlekofer K M, Bird J P, Akis R, Ferry D K and Goodnick S M 2003 *J. Phys.: Condens. Matter* **15** 147
[103] Anderson P W 1961 *Phys. Rev.* **41** 124
[104] Ng T K and Lee P A 1988 *Phys. Rev. Lett.* **61** 1768
[105] Meir Y, Wingreen N S and Lee P A 1991 *Phys. Rev. Lett.* **66** 3048
[106] Meir Y, Wingreen N S and Lee P A 1993 *Phys. Rev. Lett.* **70** 2601
[107] Wingreen N S and Meir Y 1994 *Phys. Rev.* B **49** 11040
[108] Baranger H U, Jalabert R A and Stone A D 1993 *Phys. Rev. Lett.* **70** 3876
[109] Akis R, Ferry D K, Bird J P and Vasileska D 1999 *Phys. Rev.* B **60** 2680
[110] Akis R, Vasileska D, Ferry D K and Bird J P 1999 *J. Phys.: Condens. Matter* **11** 4657
[111] Blomquist T 2002 *Phys. Rev.* B **66** 155316
[112] Connolly K M, Pivin D P Jr, Ferry D K and Wieder H H 1996 *Superlatt. Microstruct.* **20** 307
[113] Ramamoorthy A, Akis R, Bird J P, Maemoto T, Ferry D K and Inoue M submitted
[114] Bird J P *et al* 2002 *Microelectron. Eng.* **63** 277
[115] Cronenwett S M, Lynch H J, Goldhaber-Gordon D, Kouwenhoven L P, Marcus C M, Hirose K, Wingreen N S and Umansky V 2002 *Phys. Rev. Lett.* **88** 226805
[116] Meir Y, Hirose K and Wingreen N S 2002 *Phys. Rev. Lett.* **89** 196802